Contents

1. INTRODUCTION 4

2. NEED FOR THE STUDY 5

3. LITERATURE REVIEW 5
3.1. Ceria as a catalyst 5
3.2. Modification of Ceria 8
3.3. Green synthesis of metal oxide catalysts 9
3.4. Photocatalysis using Ceria 10
3.5. Malachite green dye degradation 10
3.6. Congo Red dye degradation 11
3.7. Ciprofloxacin degradation 11
3.8. Catalytic reduction of 4-Nitrophenol 12
3.9. Biginelli Reaction 15
3.10. Research problem 16
3.11. Objectives of the work 17

4. METHODOLOGY 18
4.1. Preparation of Catalyst 18
4.2. Characterization of the Catalysts 19
4.3. Statistical Experimental design 22
4.4. Catalytic reaction 23

5. RESULTS AND DISCUSSION 25
5.1. Characterization of various catalysts 25
5.2. Catalytic Reactions under study 33
5.3. Statistical Analysis of the data obtained from Box-Behnken Design 44

6. CONCLUSIONS 47

Structure of Thesis 47

REFERENCES 49

LIST OF PUBLICATIONS AND PRESENTATIONS 54
Journal Publications 54
Presentations (International & National Conferences) 55

1. INTRODUCTION

The use and importance of catalysts in chemical and industrial processes has been increasing since the beginning of 20^{th} century when oil began to replace coal as the preferred fuel in industry and automobiles. Catalysts play an important role in the conversation of energy as well as in economic development. The quest for newer and novel catalysts is always on the rise and seen as an alternative for replacing polluting processes. Among catalysts, heterogeneous catalysts make up an important type and metal oxides form an important class of heterogenous catalyst. Considerable effort has gone into developing protocols for the preparation, characterization and application of metal oxides. Of late, a lot of attention has been diverted towards Ceria (CeO_2) and Ceria based catalyst systems. Ceria based systems have found applications in diverse fields ranging from catalysis to ceramics, gas sensors, fuel cell technologies, ceramic biomaterials, solid state electrolytes etc., in addition to the classical application of CeO_2 as component in the so-called three-way catalysts (TWC) for automotive exhaust treatment. Moreover, ceria can promote steam reforming and water gas shift reactions, which count among the most researched reactions in catalytic study. The solid solutions of Ceria with transition metals and rare earth metals needs special mention for their applications in various technologically significant catalytic processes. Metal based nanoparticles possess unique properties which are markedly different and distinct from their micro sized counterparts. They find use in industry, agriculture and other household applications. Inspired by the unique and special properties of ceria, we have selected ceria-based oxides, prepared by the green or biogenic synthetic protocols for our studies. The focus for our work is the synthesis, investigation into the structural aspects and catalytic properties of pure and doped ceria-based oxide systems.

2. NEED FOR THE STUDY

The industrialized world of the present day would be unimaginable without catalysts. There is no other scientific principle which combines both economic and ecological values as well as in the study of catalysts. The development of chemical based products in advanced societies would not have been economically, technologically and ecologically possible without the use of the specific catalysts. Examples where catalysts have been used are enantiomerically pure pharmaceuticals, construction of designer polymer materials, removal of pollutants from manufacturing plants, power generating stations, motor vehicles etc. Another major area particularly relevant in the 21st century is in the production, conversion and storage of energy. With all the applications and importance of catalysts mentioned above, the quest for finding newer catalyst systems, using cheaper materials and employing environmentally benign protocols is an ongoing one. This work too in one such attempt for finding better catalyst systems.

3. LITERATURE REVIEW

3.1. Ceria as a catalyst

Rare earth elements are finding increasing applications in industry, electronics, medicine, energy and manufacturing in the chemical industry [1] . They are different from transition metals due to their unique position in the periodic table, i.e., their having 4f orbitals and the fact that they are shielded by the 4d, 5s and 5p electron make rare earth elements truly unique. The first element of the lanthanide group is Cerium, the most abundant of the lanthanides. In the field of ceria research alone around 28000 publications have been reported till date. Cerium has two stable oxidation states, +3 and +4 and can shift between these two oxidation states easily. This property is responsible for its powerful redox behavior. When combined with oxygen, Cerium forms a series of non-stoichiometric CeO_x oxide combinations with x ranging between values of 1.5 and 2 taking on a fluorite face cantered cubic (FCC) lattice. It has a cubic close packed arrangement of metal atoms wherein all the tetrahedral holes are filled with oxygen atoms. The cubic structure of ceria is found to tolerate a considerable reduction without phase change, especially at high temperatures [2].

The fluorite lattice of Ceria releases and takes in oxygen in a reversible way and this property confers unique and fascinating properties to it. This property of Ceria has been utilized in several applications ranging from catalysis [3-6] solid oxide fuel cells [7-9] where ceria increases the activity of the anode of the electrochemical oxidation, in the protection of materials [5],antioxidant agents [6], solar cells [12,13], optical films [8] gas sensors [9] and polishing agents [10] .

The wide industrial uses of nanoceria include chemical and mechanical polishing, protection from corrosion, solar cells, catalysis, and treatment of automobile exhaust. Biomedical applications of ceria are gaining much attention in the field of pharmaceuticals, drug delivery, and bio scaffolding owing to their cytotoxicity, genotoxicity, neurotoxicity, antioxidant activities (*in vivo* &*in vitro*) [12,17,18]. The bio-relevant activities comprise mimicking superoxide dismutase (SOD), peroxidase, oxidase, catalase, and phosphatase, and radical scavenging, nitric oxide radicals, and peroxynitrite [11]. The efficiency of redox-shifting between 3^+ and 4^+ states on their surface, is linked to the formation and absence of structural/surface defects namely, oxygen vacancies, and their special ability to take in and release oxygen are key components for the catalytic property of cerium oxide nanoparticles [17,19]. The remarkable antioxidant property of ceria makes them powerful candidates for their use as *in vivo* ROS scavengers, eradicate cancer cells and catalase mimicking [17, 20].

The suitable band gap (3.19 eV) and the prominent electronic (n-type semiconductor) and optical property that CeO_2 exhibit makes them strong candidates for photo-degradation of organic dyes from industrial wastewaters. The photocatalytic process involves the separation of charges (electrons and holes) in the semiconductor system by the absorption of light with appropriate wavelength. The photogenerated electrons and holes release reactive oxygen species from the aqueous environment thereby react with organic dye molecules and decompose them [14].

Recent reports illustrate that the reactions where hydrogen is generated, like ethanol reforming or water-gas shift process catalyzed by transition metals can be improved using ceria as support material. The CeO_2 support provides good dispersion for the metal catalyst, thereby increasing its stability [15] The relevant example includes Ni/CeO_2 system where the beneficial behavior of

rare earth oxides in the ethanol steam reforming reaction is indicated and exhibits good activity, stability and hydrogen selectivity [16].

One of the modern ceria based photocatalytic system contains ceria-titania composite materials. It is reported to have enhanced activity towards the decontamination of Volatile Organic Compounds. The disadvantages such as wide band gap, low sunlight absorption and instability of conventional photocatalysts like TiO_2 can be overcome using this composite. In terms of catalytic output, ceria-titania (CeO_x-TiO_2) composite materials have shown excellent photodegradation performance against a notable number of pollutants under several conditions [17].

The enhanced catalytic performance, due to the synergistic combination of metal and ceria was established by Tang et al. [18]. Tang and co-workers recently reported the synthesis and properties of Pt decorated ceria nanoflakes using atomic layer deposition process. The prepared nano-array monolithic Pt/CeO_2 showed increased catalytic oxidation reaction towards gases like propylene, propane, CO, and NO with almost 90 % conversion efficiencies at temperatures below 200 °C. Cerium oxide is a highly useful component in three-way catalysts and in oxidation diesel soot in modern exhaust after-treatment devices due to its remarkable oxygen storage capacity and thermal stability. Alternatively, ceria is an important ingredient in materials used in gas sensing, water oxidation, photo-catalysis, water-gas-shift reaction , reduction of CO_2, and purification of water [19].

In 2018 Lykaki et al. [13] studied the unique synergistic effects arising out of metal-support interactions by combining ceria with transition metals and observing its electronic, geometric and bifunctional interactions between both the components and compared this with bare oxides. The synergistic effect was found to be the best in Cu/CeO_2 system and studied in three different ceria nanostructures (rods, polyhedra, cubes).

Another modern-day application of CeO_2 explained by Magudieswaran et al. [20] is about the economic yet simple way of removing pollutants from indoor air through photocatalytic oxidation. They utilized the specific properties of ceria such as Ce^{4+}/Ce^{3+} redox couple formation, high resistance to chemical and photo corrosion.

The oxygen vacancies could promote the preferential oxidation of CO for hydrogen purification, water gas shift (WGS) reaction and several other reactions. Pizzolitto et al. [21] successfully demonstrated catalytic application of the ternary system which contains nickel, ceria and lanthanum. The attractive properties of doped ceria come from the increase in the number of oxygen vacancies during doping process. Zagaynov et al. [22] successfully synthesized ceria doped with Cu, Mn and Zr using co-precipitation method. The relationship between physicochemical properties of mesoporous metal oxides that enhances the oxygen vacancies, redox properties, stability, and, significantly catalytic activity was detailed in this paper.

3.2. Modification of Ceria

While Ceria has several properties, which are special and unique, it also suffers from some drawbacks. Ceria has a poor thermal stability, it suffers from low surface area, is prone to sintering easily and its poor catalytic efficiency in the pure state make it difficult to be used as a catalyst. Modification of a catalyst improves the stability of a catalyst and prevents it from sintering, it is true for Ceria also. Further modification of ceria also can have a positive impact on its catalytic activity. Rare earth elements are finding increasing applications in industry, electronics, medicine, energy and manufacturing in the chemical industry [1] . They are different from transition metals due to their unique position in the periodic table, i.e., their having 4f orbitals and the fact that they are shielded by the 4d, 5s and 5p electron make rare earth elements truly unique.

Combining two metal oxides can lead to structural changes, improve their reductive abilities and its oxygen migration capabilities, all of which will have an impact on its catalytic efficacy. The second metal oxide can also increase the number of defects by producing strain on the host lattice. It has been reported that the mixed oxides of hafnia and ceria prepared using the citric acid (Pechini method), forms solid solutions with improved phase stability and redox properties. Further, Devaiah et al have synthesized a series of mixed metal oxide catalysts with ceria as one of the components along with other rare earth metal oxides like zirconia, hafnia, praseodymia, lanthana etc. all modified by the co-precipitation method. Mixed La_2O_3–CeO_2 have received a lot of attention due to their increasing applications in catalysis, absorption and other related areas.

There has been reports of doped lanthana nanoparticles exhibiting chemical stability and photoluminescent behavior. Doped ceria has shown improved performance as a catalytic support and oxygen storage capacity in important applications such as automotive exhaust control. Among the various mixed oxides of ceria, the most important is ceria-zirconia. Ceria–zirconia solid solution has been reported to show high thermal stability, enhanced catalytic properties and oxygen storage capacity.

3.3. Green synthesis of metal oxide catalysts

According to Cheviron et al. [23], solvent medium, non-toxic reducing agents, and environmentally safe nanoparticle stabilizers are the three aspects that need to be addressed in green synthesis:. Cruz et al. have stated that green synthesis by plant extracts can be comparable to some of the classical methods; however, aspects such as yields, stability, and ions reduction mechanisms have not been explained well. The large scale production of atomically precise metal nanoparticles require very reactive substances and/or energy intensive procedures, both of which don't qualify as environmentally friendly [31,32]. To overcome this problem, researchers have begun to adopt environmentally benign methods, collectively referred to as green synthesis. A simple search using the keywords ''green synthesis + metal nanoparticles'' showed more than 30,000 results as research article alone, while Sc Finder Scholar showed more than 1600 results (January 2019). Moreover, there has been a steady increase in publications since 2006. The biological synthesis of metal and metal oxide nanoparticles has been accomplished using microorganism in addition to plants [33,34]. A thorough review on the synthesis of MNPs by microbes is provided by Narayanan and Sakthivel [28], Hulkoti and Taranath [29] and Virkutyte and Varma [30]. Reports of the reduction of precious metals by inactivated plant materials go back to more than 100 years. Molisch and Iwase have studied the reduction of silver by chlorophyll from plants and the reduction of gold using the extract of fresh leaves, respectively. About 70 years ago, Nagai et al reported the reduction of Ag $(NO)_3$ using plant cells. More than a decade ago, Armendariz et al. [31] reported the reduction of $KAuCl_4$ using powdered wheat (*Triticum aestivum*) and oat (*Avena sativa*) biomasses and the subsequent formation of Au NPs. These researchers have reported that the solution pH is a key variable that influences the size and to reduce the polydispersity of the biogenic Au NPs. Water extracts of alfalfa (Medicago sativa) biomass led to the formation of triangular nanoplates, while isopropyl alcohol extract rendered

decahedra and icosahedra NPs [32]. Besides biomass, living plants can also reduce KAuCl4 and form metal NPs. Gardea-Torresdey et al. [31,40] reported, the formation of metal NPs by living plants exposed to $AuCl_4$ - solution. Alfalfa plants were grown in an agar medium doped with $AuCl_4$ - and formed crystalline pure Au NPs, showing that the NPs grew within the plant [33]. Thousands of papers have appeared mentioning the formation of MNPs by plant or plant-derived materials. Detailed information can be found in Hong et al. and Virkutyte and Varma [25].

3.4. Photocatalysis using Ceria

There has been a huge interest in the field of photocatalysis, for visible-light water splitting, mineralization of organic pollutants in wastewater etc. While the number of semiconductor metal oxides that show good photocatalytic activity under illumination of visible-light is still limited, the fact remains that most of these studies are carried out with modified TiO_2 based systems [34]. Kashinathan et al. have studied the photocatalytic degradation of the dye RhB using solar irradiation over CeO_2 doped TiO_2 nanocomposites that was synthesized hydrothermally [35]. A novel method to improve significantly the photocatalytic efficiency in mesoporous nanorod-like ceria by coupling oxygen ion conduction to photo catalysis has been reported by Yuanzhi Li et al. [36].

3.5. Malachite green dye degradation

Malachite green dye is used to dye materials like silk, paper and leather. Both malachite Green (MG) dye and its reduced form have shown to have adverse effect on reproductive and immune system. It is used as a food coloring additive, as a dye in fabrics, paper, leather and acrylic industries. Wastewater containing this dye emerging from textile mills appears deeply colored and is shown to be carcinogenic. Hence it is important to treat the waste water before its discharge into the water body. One of the commercial and simple methods of waste water treatment is the photocatalytic degradation process which deteriorates all the toxins in the effluent through advanced oxidation process. Photocatalytic degradation is conducted by irradiating the aqueous dye solution in the presence of photocatalysts and light of appropriate wavelength. Some of the common photocatalysts used for this purpose are titanium dioxide (TiO_2), zinc oxide (ZnO) [37].

Photocatalytic degradation study using EDTA capped ZnO nanomaterials showed more than 90% degradation of MG dye in aqueous solution [38]. ZnO nanosized sol–gel thin films are also promising and efficient catalyst for photocatalytic degradation of MG [39].

3.6. Congo Red dye degradation

Congo red (CR), a well-known dye, which is used to prove the presence of myloidal deposits in tissue. CR is of interest for more than a 100 years for its use in investigation in neuropathology [40]. Congo red is shown to be toxic. Reports show that CR can reduce serum protein concentration and cause disseminated micro embolism, platelet aggregation and thrombocytopenia.

3.7. Ciprofloxacin degradation

In the field of pharmaceuticals fluoroquinolone group make up one of the most significant class of compounds used globally for humans and veterinary purposes. The presence of fluoroquinolones in waste water is reported in many countries. The challenge posed by these compounds is because it cannot be fully metabolized by the body and so has to be excreted and enters the environment through wastewater effluents. Thus, development of alternative physiochemical technologies is needed to mitigate such discharges into the environment. Heterogeneous photocatalysts were proposed as a suitable advanced technology for the degradation of fluoroquinolone [41].

Babić et al. [42] shown that solar irradiation plays a significant role in the degradation of three fluoroquinolone derivatives, ciprofloxacin, norfloxacin, and enrofloxacin found in river and industrial wastewater. And their results proved that photodegradation can be an important way to eliminate these substances from wastewater. It has been shown that photodegradation is possible elimination process for fluoroquinolones from the environment. Detailed studies on the photochemistry of the intermediates are required because of the several steps involved and the role played by conditions.

Various visible-light-driven (VLD) semiconductor materials, such as bismuth-based semiconductors, rare earth metal oxides, noble metal-based semiconductors, and even non-metal-

based graphitic carbon nitride have been found effective for heterogeneous photocatalysis. It was reported that CeO2–Ag/AgBr composites have shown good photocatalytic activity for the photodegradation of ciprofloxacin under visible light irradiation [43].

Gad-Allah et al. [44] used a simple, safe, cheap, photostable, and very photoactive titanium dioxide photocatalyst for the degradation of ciprofloxacin. And they achieved good results at low pH condition and high catalyst concentration.

Qian et al. [45] successfully synthesized $CeO_2/NaNbO_3$ heterostructure composites and the degradation ability of this system was much better than pure $NaNbO_3$ under UV light irradiation. Nekouei et al. [46] synthesized Ag/AgCl N-doped activated carbon nanocomposite catalyst for the first time and this was successfully utilized for the catalytic oxidation activities for ciprofloxacin removal in aqueous solution. Liang et al. [47] successfully fabricated Ag-assisted heterojunction composite AgBr/Ag, Ag_2O/Ag_2CO_3 and showed high charge pair separation efficiency and thereby remarkable photocatalytic degradation towards ciprofloxacin. Rahmani-Aliabadi et al. [48] used coupled FeS-Fe_2S_3 supported onto the zeolite nanoparticles to study the degradation of ciprofloxacin. The better charge transfer in the coupled system enhanced its photocatalytic activity.

3.8. Catalytic reduction of 4-Nitrophenol

The lethal effects of nitrophenols (NPs) on environment and health was first reported 40 years ago. Nitrophenols are a class of compounds that can inhibit the oxygen carrying capacity of blood and they are identified as potent vasodilators. Headache, nausea, fever, shortness of breath, and numbness are the common symptoms of exposure to NPs. In plants, some NPs directly attacks the cell metabolism, even at very low concentrations by uncoupling oxidative phosphorylation, decreasing transpiration and inhibit absorption of nutrients and growth. This finally leads to forest decline and worse at a later stage. NPs are also lethal to aquatic life (algae and fish). Common sources for NPs consist of industrial raw materials or intermediates involved in the pharmaceuticals, manufacturing of plastics, dyes, explosives, disinfectants, herbicides, and insecticides combustion of coal and wood, and mainly, internal combustion engine exhaust etc.[49].

Considering the harmful effects of NPs many methods were employed for its removal from the environment. Some previous methods involve adsorption, photocatalytic degradation, catalytic oxidation, microbial degradation, microwave-assisted, electro-Fenton method, electrocoagulation, electrochemical treatment and so on. In contrast to the adverse effects of 4-NP, its reduced product, 4-aminophenol (4-AP) is an important intermediate for the manufacture of analgesic and antipyretic drugs. But direct hydrogenation of 4-NP requires high temperature and pressure condition. So much attention was drawn into this reduction reaction and many attempts were carried out to make this reaction feasible and fast under mild conditions in aqueous medium.

The industrial importance of 4-AP and derivatives accelerated the study of catalytic reduction of 4-NP. The reaction mechanism of nitroarene reduction was proposed by Haber 100 years ago. The mechanism involves the presence of number of reactive intermediates and the final aniline product comes after several complex steps. And one of the unwanted byproducts of the reaction is hydroxylamine and if the activity of the catalyst is low, accumulation of hydroxylamine occurs. The slow activity of the catalyst and accumulation of hydroxylamine can be reduced using promoters, especially of vanadium compounds [50].

The reduction of 4-NP with $NaBH_4$ is a six-electron transfer process. The peak due to 4-NP was red shifted from 317 to 400 nm when $NaBH_4$ was added to the aqueous solution due to the formation of 4-nitrophenolate ions under alkaline conditions [51]. Till today, this reaction stands as a standard to assess the quality and catalytic performance of any catalyst nanoparticle. The catalytic reduction reaction should be simple yet trustworthy and should have a wide appeal so that the reaction can be studied with certainty employing a simple experimental set up. The progress of 4-NP to 4-AP can be monitored at different time intervals using UV -Visible spectrophotometry. Under suitable experimental condition the reaction passes through two distinct isobestic points and produce only 4-aminophenol without any side product. The final product (4-AP) is valuable in pharmaceutical industries for the manufacture of analgesic, antipyretic and other drugs, corrosion inhibitor, in photographic developer, anticorrosion lubricant etc. Also functionalized 4-AP and its derivatives are widely used for the production of polymers, herbicides and other chemicals [52].

Heterocatalysis using nanoparticles have emerged as viable, easily available method for the reduction of 4-NP in the presence of $NaBH_4$. The kinetics of heterogeneous catalytic reduction of 4-NP was successfully demonstrated by Wunder et al. [53]. The catalytic reduction of 4-NP using Pt, Au nanoparticles can be modeled in terms of the Langmuir-Hinshelwood model which assumes that adsorption of both reactants onto the surface of the catalyst. In terms of catalytic reusability and stability in aqueous medium, Au nanoparticles supported on the magnetic nanocarrier serves this purpose in an efficient way [54]. Jana et al. [51] exhibited the efficiency of resin-bound silver nanocomposites for the reduction of 4-nitrophenol in the presence of ice-cold, freshly prepared aqueous solutions of $NaBH_4$. Kong et al. [55] gave a new explanation for the mechanism of nitro to amino groups conversion. The proposed that the hydrogen atoms in the reduced product (4-AP) comes from H_2O based on the isotopic analysis, rather than $NaBH_4$ and the role of $NaBH_4$ is to bring H^- ion which will break the original hydrogen balance in the solution and help H_2O produce H^+, facilitating their adsorption onto the nitro groups thus promoting the reaction to proceed. Kong et al. [56] successfully developed N-doped graphene, a metal free catalyst using the excellent physical, chemical and mechanical properties of graphene. And this material showed promising result in the reduction of 4-NP using $NaBH_4$. Li et al. [57] synthesized self-assembled of Au/graphene sheets under hydrothermal conditions and showed its catalytic ability towards the reduction of 4-NP to 4-AP. The high adsorption power of graphene and the efficient electron transfer to Au enhances its catalytic capacity and this makes the Au/graphene hydrogel an efficient catalyst in the reduction of nitroaromatic compounds. Morales et al. [58] recently attracted the attention of researchers Cu-Pd catalysts supported on high surface area graphite which showed excellent catalytic activity towards the reduction of 4-NP with remarkable high stability after several cycles. And the Cu dispersed graphite catalyst was able to show 100 % 4-NP reduction with less time compared to N-doped carbon nanofilm, carbon composite microspheres and reduced graphene oxide. Sharma et al. in [59] introduced cobalt doped CuO nanoparticles which could complete the reduction in merely 3 minutes in the presence of $NaBH_4$ as reducing agent. The transition metal doping can result in decreases in particle size and subsequent enhancement of catalytic activity. Shen et al. [60] prepared uniform spherical gold nanoparticles (AuNPs) with good dispersity and stability using biogenic AuNPs cell-free extracts of *Aspergillus sp*. WL-Au.

This was found to be more economically viable, cost-effective and eco-friendly method for the synthesis of AuNPs which has already proved to be the best catalyst for nitroarene reduction. Yusran et al. [61] developed a novel catalyst from cheap, facile and simple method and prepared Cobalt nanocatalyst series by the direct carbonization of Cobalt-Metal Organic Framework. Metal Organic Framework is tunable and possess better catalytic properties such as high surface area, low density, functionalizable and controllable size and morphology during synthesis. And it is interesting to note that this material gave an excellent catalytic efficiency towards the complete conversion of 4-NP to 4-AP in 45 seconds.

3.9. Biginelli Reaction

In 1881, Arthur Hantzsch [62] performed the first synthesis of a dihydropyridine. The three component Biginelli reaction was first proposed by Italian chemist Pietro Biginelli [63] in 1893. He reported an acid catalyzed cyclocondensation reaction of acetoacetic ester, benzaldehyde, and urea dissolved in ethanol with a small amount of HCl under reflux conditions. The precipitated product of this novel one-pot, three-component synthesis was proposed correctly by Biginelli as 3,4-dihydropyrimidin-2(1*H*)-one. Biginelli reaction is a multicomponent reaction which yields a 3,4-dihydropyrimidinone product that exhibit potential pharmacological activity. Products of Biginelli reaction have been identified as a new class of calcium channel blockers. A classic reaction involves the one pot synthesis of 3,4-dihydropyrimidinone using an aldehyde, a β-keto ester, and urea as reactants. Modified Biginelli reaction protocols are now available for students to carry out under laboratory settings and the yields ranged from 20 % to 80 %, averaging 58 %. The high melting point and low solubility of the product make it easy to be isolated [64]. Kappe's experimental evidence shows the acid-catalyzed condensation of benzaldehyde and urea leading to a hemiaminal, which dehydrates to form a key N-acyliminium ion intermediate. The enol form of ethyl acetoacetate attacks the N-acyliminium ion to generate an open chain ureide, which then cyclizes to form the product, dihydropyrimidine. And this is the mechanism that is most widely accepted for the Biginelli reaction [65].

Later, it was found that applying the modifications of the Biginelli reaction to the Hantzsch synthesis too gave very good results. A good yield was obtained when the reactions were performed over both acidic and neutral alumina. Better results were obtained when reactants

under neat conditions were subjected to microwave irradiation. Kidwai et al. [66] developed a simple, economical and environmentally benign synthesis that involves microwave irradiation of the reactants (acetoacetic ester, aldehyde and ammonium acetate). Thus, solvent free Biginelli synthesis gained more attention and this can minimize solvent pollution. Modification and improvements of the Biginelli reaction products were reported using Lewis acids such as $BF_3.OEt_2$,$FeCl_3$ and HCl, $LaCl_3.7H_2O$, $La(OTf)_3$, $Yb(OTf)_3$, $ZrCl_4$, $BiCl_3$, $Mn(OAc)_3$, $LiClO_4$, H_3BO_3 and polyphosphorate ester to enhance the yields and minimize reaction conditions [67].

3.10. Research problem

Even though ceria, as has been reported widely, been synthesized, as single oxide, mixed oxide and in modified forms, using different methods, not many methods produce ceria in the nano dimensions. Only sol-gel method gives the ceria in the nano dimensions, but it has the problem of being time consuming and uses expensive chemicals like isopropoxides. To the best of our knowledge, modified ceria nanoparticles has not been prepared using the solution combustion synthesis using plant extracts as fuel using the green route.

Among the photo reduction reactions, mostly titania and modified titania were being used till now, we would like to investigate the photo reduction ability of ceria, which has a band gap similar to that of titania. Further, it would be very significant if some work can be done where Ceria and modified Ceria are used in areas where pollution abatement is involved; degradation of the drug Ciprofloxacin, dyes like Malachite Green and Congo Red can all be degraded using novel catalyst systems. Though many catalyst systems are there, the quest for a more economic, quicker and cleaner alternative is an ongoing one.

3.11. Objectives of the work

- To prepare Ceria and modified Ceria nanoparticles using plant extract by solution combustion synthesis. The various plant identified are namely, *Musa paradisiaca, Scutellaria barbata, Sesbania drummondii* and *Acalypha indica* and optimizing any one of the four plants.
- Modification of Ceria using f block and d block elements (Sm, La, Zn, Ti, Ag, Bi) and to investigate the surface characteristics of the catalyst systems using various spectroscopic and non-spectroscopic techniques namely XRD, FTIR, SEM, XPS, TEM, DLS and Raman spectroscopy.
- To evaluate the catalytic activity/efficacy of the prepared catalysts on the following reactions. a) Photochemical degradation of the dye Malachite Green and Congo Red. b) Degradation under sunlight of the drug Ciprofloxacin c) reduction of 4-nitro phenol d) synthesis of compounds using the Biginelli synthesis.

Plan of Work

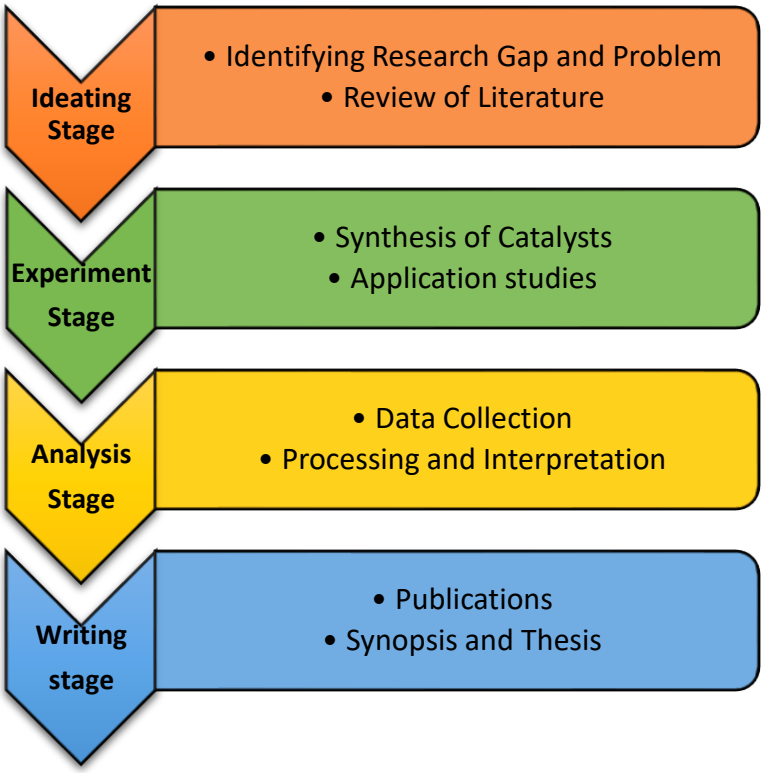

4. METHODOLOGY

4.1. Preparation of Catalyst

There are many methods of preparation available for catalysts, and solution combustion synthesis is one of the most convenient methods. The principle behind this method is that once a reaction is initiated by heating, an exothermic reaction is initiated, which, within a short period of time becomes self-sustaining, leading to the final product in the form of a powder. This method of synthesis has the advantage of producing fine and homogeneous powders within a short period of time. Since it is an exothermic and self-propagating process, produces a high amount of heat, and can sometimes be explosive and adequate precautions should therefore be undertaken.

Synthesis

Fresh leaves are taken, cleaned, washed and dried. The leaves are shredded and refluxed for 30 minutes with water in a round bottom flask. The resulting solution is filtered, and calculated amounts of cerium nitrate is added to the filtrate and combusted in a muffle furnace preheated to 400° C and maintained at that temperature for 5 hours. The powder obtained after combusting is then ground finely using a mortar, weighed, labelled and stored in a desiccator. The amount of cerium nitrate is calculated to obtain different weight percentages. The schematic diagram for the preparation of the catalyst is given in Figure 1 and different plant systems were tried are given in Table 1. Table 2 gives the various catalysts prepared in the present study.

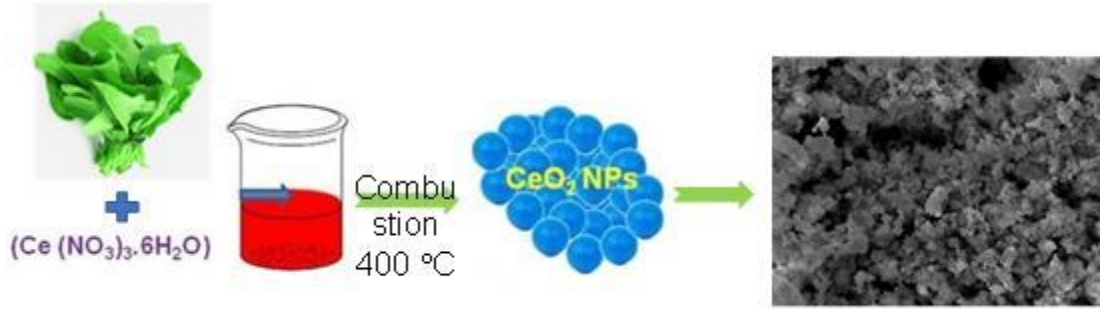

Figure. 1: Schematic diagram of the preparation of ceria-based catalyst

Table 1: Plant systems used for optimization

Plant	**Botanical Name**
Plantain leaf	*Musa paradisiaca*
Bay leaf	*Laurus nobilis*
Spinach leaf	*Spinacia oleracea*
Spinach leaf (extract)	*Spinacia oleracea*
Betel leaf	*Piper betle*

Table 2: Different catalyst systems prepared

Catalyst system	**Composition**	**Name**
CeO_2		C100
CeO_2:Sm_2O_3	85:15	CS 101
CeO_2:Sm_2O_3	90:10	CS102
CeO_2:Sm_2O_3	95:5	CS103
CeO_2:La_2O_3	85:15	CL 101
CeO_2:La_2O_3	90:10	CL 102
CeO_2:La_2O_3	95:5	CL 103
CeO_2:Sm_2O_3: La_2O_3	90:05:05	CSL101
CeO_2:TiO_2	50:50	CT101
CeO_2: ZnO	85:15	CZ 101
CeO_2: Ag	99.9: 0.1	CA101
CeO_2: g C_3N_4	50: 50	CG101
CeO_2: Ag: g C_3N_4	49.95: 49.95: 0.1	CAG101

4.2. Characterization of the Catalysts

4.2.1. X-Ray Diffraction Analysis:

XRD is a reliable and indispensable techniques in characterization of a catalyst. It helps in identifying parameters like crystal structure, crystallinity, phase purity, and crystallite sizes of

catalyst materials. The structure of all the nanoparticles was elucidated using a Bruker AXS X-ray diffractometer in the 2θ range of 5 to 80° (Cu Kα radiation source, λ=1.541 Å). Interpretation of the XRD data is done by comparing the spectrum obtained with a standard spectrum, taken from any X-ray powder data file catalogues, published by the American society for testing materials (JCPDS).

4.2.1. Infra-Red Spectroscopy:

Fourier transform infrared (FT-IR) spectroscopy is used by chemists to determine the functional groups found in compounds. Each atom of a molecule is connected by bonds and each bond vibrates with a different frequency, all within the IR region so characteristic peaks are observed at different frequencies, depending on the elements and types of bonds. The type of bonds present in the sample was analyzed using FTIR spectroscopy (Prestige 21, Shimadzu). The changes in the absorption bands were studied in the range 400-4000 cm^{-1}.

4.2.2. Raman Spectroscopy

Raman spectroscopy is extensively used in the study of oxides, supported oxides, supported and bulk metals, and has steadily found increasing applications in characterizing supported transition metal oxide catalysts. It is based on the inelastic scattering of photons, which are incident on the sample. The crystal structure and vibrational mode of the prepared catalysts can be confirmed with the help of Raman spectroscopy *HR-Lab Raman*.

4.2.3. UV–vis diffuse reflectance spectroscopy

UV Diffuse reflectance spectroscopy (DRS) throws light into the interactions of the catalyst with photons of different frequencies. The fundamental absorption, determined in this method, corresponds to the excitation of the electron from the valence band to the conduction band, which can then be used to calculate the nature and value of the optical band gap. UV-vis DRS spectrum was recorded using *Shimadzu MPC3600* spectrometer in the wavelength range of 200 to 800 nm using $BaSO_4$ as standard. Kubelka-Munk method was used to calculate the band gap energy of the samples.

4.2.4. Thermal Analysis

Thermal methods are used to study the relationship between temperature and the property of a system. Heat of reaction and volume are some of the properties studied. In a thermo gravimetric analysis (TGA), the mass of sample is recorded continuously while its temperature is increased continuously at a predetermined rate beginning from room temperature to a high temperature. TGA and DSC were recorded using *SDT Q600- TA* Instrument with a heating rate of 20°C/min.

4.2.5. Scanning Electron Microscopy and Elemental Analysis

Scanning Electron Microscopy (SEM) is one of the most advanced techniques available for characterizing the size and morphology of catalysts besides providing other topographical information. Morphological analysis of the sample was carried out using the SEM-EDAX in a *FEI Inspect S50* scanning electron microscope.

4.2.6. Transmission Electron Microscopy (TEM)

Transmission Electron Microscopy (TEM) is typically used to obtain high resolution images of a solid sample for nanostructural and compositional information. Morphological analysis of the sample was carried out using the SEM-EDAX using a *FEI Inspect S50* scanning electron microscope and TEM using *Titan Themis 300kV* Transmission Electron Microscope from *Thermo*.

4.2.7. Dynamic light scattering

Dynamic light scattering (DLS), also referred to as Quasi Elastic Light Scattering (QELS), is a simple, non-invasive, light scattering technique, used for measuring the size and size distribution of and particles typically in the submicron region, but with recent advances, lower than 1nm. Our studies were conducted on a *Horiba, SZ-100 Nanoparticle Analyzer*.

4.2.8.X-ray photoelectron spectroscopy

X-ray photoelectron spectroscopy which is yet another advanced technique and is generally used to study the composition of the surface and the oxidation state of the elements on the surface. In

our studies, *Omicron Nanotechnology XPS* system was used with a monochromatic Al Kα radiation (hυ = 1486.6 eV) of source voltage 15 kV and emission current of 20 mA. The scans were carried performed at a high vacuum of 2×10^{-10} mbar. The obtained XPS spectra were de convoluted using *Casa XPS* program, wherein the background was simulated using the Shirley function and the peaks were fitted using a Gaussian Lorentzian function. All binding energies were referenced to C1s for calibration.

4.3. Statistical Experimental design

The statistical software *Minitab version 18 (Minitab USA*) was used for designing and analyzing the effect of various reaction parameters towards 4NP reduction. Box-Behnken experimental design (BBD) along with RSM was used to understand the different interactions among the variables and the corresponding responses. The model used here was for arriving at a statistical and mathematical correlation between different independent variables on the extent of dye degradation. To minimize errors, 27 trials were executed, all in duplicate, and the % of 4NP reduction was taken as the response variable. The relationship between the response and independent variables is explained by the quadratic polynomial equation (Eq. 1) on which the model is based [75,76].

$$Y = \beta_0 + \sum_{i=n}^{n} \beta_i X_i + \sum_{i=j}^{n}\sum_{i=j}^{n} \beta_{ij} X_i X_j + \sum_{i=n}^{n} \beta_{ii} X_i X_i , \qquad i < j \tag{1}$$

Where Y stands for response variable, β_0, β_i, β_{ii} and β_{ij} stand for interception coefficient, coefficient of the linear effect, coefficient of quadratic effect, coefficient of interaction effect respectively when i< j. Total number of variables are represented by n. The analysis of variance *(ANOVA)* of the model is also done using the same software Minitab. To check the validity of the quadratic model, predicted by the software *Minitab 18,* few experiments as were performed.

4.4. Catalytic reaction

4.4.1. Photocatalytic Degradation of Malachite green (MG)

Photocatalytic degradation experiments using the prepared CeO_2 based catalysts have been studied by malachite green (MG) dye under visible light. In a typical experiment, 50 mL aqueous solution of malachite green (MG) dye, was taken along with the catalyst was stirred in the dark for 15 minutes to establish adsorption-desorption equilibrium of the dye with the catalyst. This solution was then exposed to visible light in a photoreactor while keeping the reaction mixture stirred for agitation. The absorbance of the solution was recorded every 10 min at 616 nm of light irradiation using UV–Vis spectrophotometer. The analysis was done using a *Shimadzu UV-Vis 1800* spectrophotometer from 400 to 800 nm. The extent of degradation of the dye was then calculated in using the formula given in Eq.2.

$$\%\, degradation = \frac{(C_0 - C)}{C_0} \times 100 \qquad (2)$$

Where C_0 and C are the concentrations of the dye before and after irradiation

4.4.2. Photocatalytic degradation of Congo red (CR)

The photocatalytic efficiency of the prepared catalysts was evaluated on the second dye, Congo Red (CR) in addition to the MG dye mentioned above. In a typical experiment, 50 mL aqueous solution of Congo red (CR) dye (20 mg/L) was taken along with the catalyst (0.1g) was stirred in the dark for 15 minutes to establish adsorption-desorption equilibrium of the dye with the catalyst. This solution was then exposed to visible light (direct sunlight) in a photoreactor while keeping the reaction mixture stirred for agitation. The absorbance of the solution was recorded every 10 min at 616 nm of light irradiation using UV–Vis spectrophotometer. The extent of degradation of the dye was then calculated in using the formula given in Eq.2 given above.

4.4.3. Photocatalytic degradation of Ciprofloxacin

The prepared catalysts were studied for the degradation of the antibiotic drug, Ciprofloxacin. The drug solution was mixed with the photocatalyst and stirred for about half an hour to attain

absorption desorption equilibrium between the drug and catalyst. The lamp was then switched on and at regular intervals of irritation, definite volumes of the solution was drawn out, centrifuged to remove the photocatalyst and then placed in the UV-vis spectrophotometer to record the absorbance at λmax=276nm. The procedure was continued till complete degradation took place. Trials were repeated by varying parameters like concentration of catalyst, concentration of ciprofloxacin and pH. Based on the valued obtained before and after irradiation process viz., A_o and A_t, respectively, C/C_0 values were calculated to obtain the efficiency of degradation. All readings were taken in triplicate, and the values were averaged to ensure accuracy.

The light source was a 30W UV lamp. In a typical experiment, 10 mg of catalyst was added into CIP (100 mL, 3 μM) solutions. After commencement of irradiation, an approximately 5.0 mL suspension was taken out, centrifuged and separated at given time intervals to obtain the supernatant liquids.

4.4.4. Catalytic Reduction of 4-nitrophenol (4-NP)

The catalytic reduction of 4-NP to 4-AP using $NaBH_4$ was carried out in the presence of the prepared catalysts. The reaction process was monitored by Shimadzu UV1800 UV-Vis spectrometer. 100 ml of 0.2 mmol of 4-NP was freshly prepared from 5 mmol stock solution of 4-NP. The UV-vis spectrum was recorded before and after the addition of $NaBH_4$(500 mg). Addition of $NaBH_4$ to 4-NP resulted in a gradual color change from pale yellow to yellowish green. Subsequently, 100 mg of the catalyst was added. As the reaction proceeds the solution gradually became colorless from yellowish green color. The kinetics of the reaction was monitored by the decrease in the intensity of the absorption peak at 400 nm at different time intervals. To determine the stability and reusability of the prepared catalyst over 4 cycles, the used catalysts was centrifuged at 6000 rpm, washed with water, dried at 50 °C and activated after each cycle.

4.4.5. Biginelli reaction

To a 10-mL r.b. flask fitted to a reflux condenser benzaldehyde (254 μL,266 mg, 2.5 mmol), ethyl acetoacetate (500 μL, 496 mg,2.8 mmol), urea (150 mg, 2.5 mmol) and 1.0 mL of 95%ethanol and boiled under reflux conditions for 90 minutes. The reaction flask was cooled to

0 °C and the resultant precipitate was filtered and washed with cold ethanol. The product (120–520 mg, 20–80%, average yield 189 mg, 58%; lit. yield 78.5%) was obtained as a white solid, with a typical m.p 198–200 °C (actual m.p 202.4 °C).

5. RESULTS AND DISCUSSION

5.1. Characterization of various catalysts

XRD analysis of ceria prepared using different plant extracts are shown in Figure 2. All the plots indicate the formation of cerium oxide with standard fluorite structure. The planes (111), (200), (220) and (311), indicate the characteristic face centered cubic phase of CeO_2 and correspond to the 2θ values 28.2, 32.7,47.1 and 55.9 respectively [68]. From the plots, the one with the spinach leaf (*Spinacia oleracea)* were found to be the most crystalline and having the smallest crystallite size. Further, on investigating the dye degradation studies with Malachite Green catalysts (discussed later), the same catalyst system was found to be the most efficient. Thus,

the catalyst system prepared from the green spinach leaf (*Spinacia oleracea)* was chosen and all further catalyst systems were prepared using this leaf.

Modified forms of catalysts prepared using the plant extract also shows the same characteristic peaks of cerium oxide. In the XRD plots of the modified catalysts, Figure 3, the peaks of the doped metal oxides do not show up indicating the dopants are present in quantities that are not large enough to show up in the XRD pattern.

The Debye Scherrer equation (Eq. 3) can be applied to find the average crystalline size [69, 78].

$$D = \frac{k\lambda}{\beta \cos\theta} \qquad (3)$$

D is average crystalline size, β is line broadening in radius, θ Bragg angle and λ is x-ray wavelength (0.1541 nm for Cu-Kα). k is a constant and it is usually taken as 0.94. The values of β and θ are determined from the prominent peak at $2\theta=28.3^0$. The crystalline size of the nanoparticle was found to be 80 to 100 nm calculated using Eq (3) for various catalysts.

The d spacing of each plane can be calculated using the Bragg's equation (Eq 4) and lattice parameter of the nanoparticle can be estimated from Eq (5). Calculated value for the lattice parameter is closely related to the standard value.

$$n\lambda = 2dsin\theta \tag{4}$$

$$\frac{1}{d_{hkl}^2} = \frac{a^2}{h^2 + k^2 + l^2} \tag{5}$$

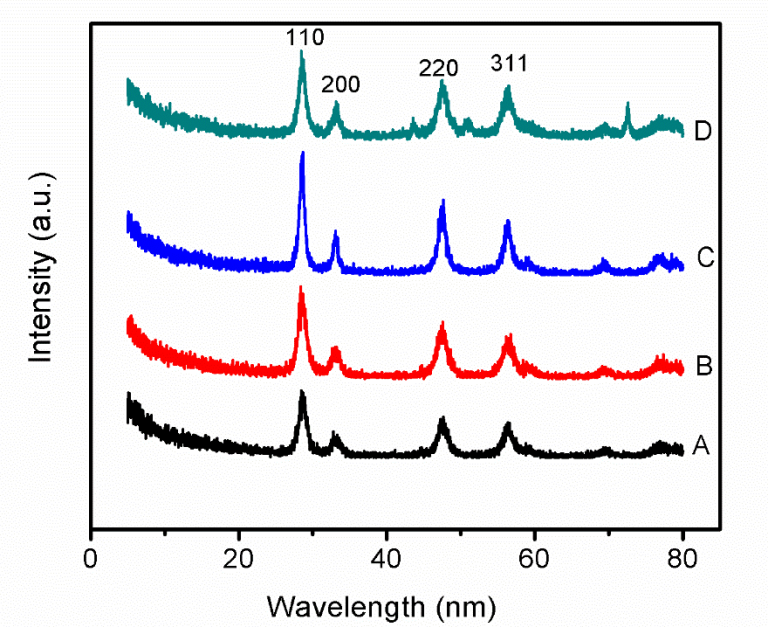

A: Plantain leaves B: Bay leaves C: Spinach leaves D: Palak leaves extract

Figure 2: XRD pattern of Cerium oxide prepared using different leaf extracts

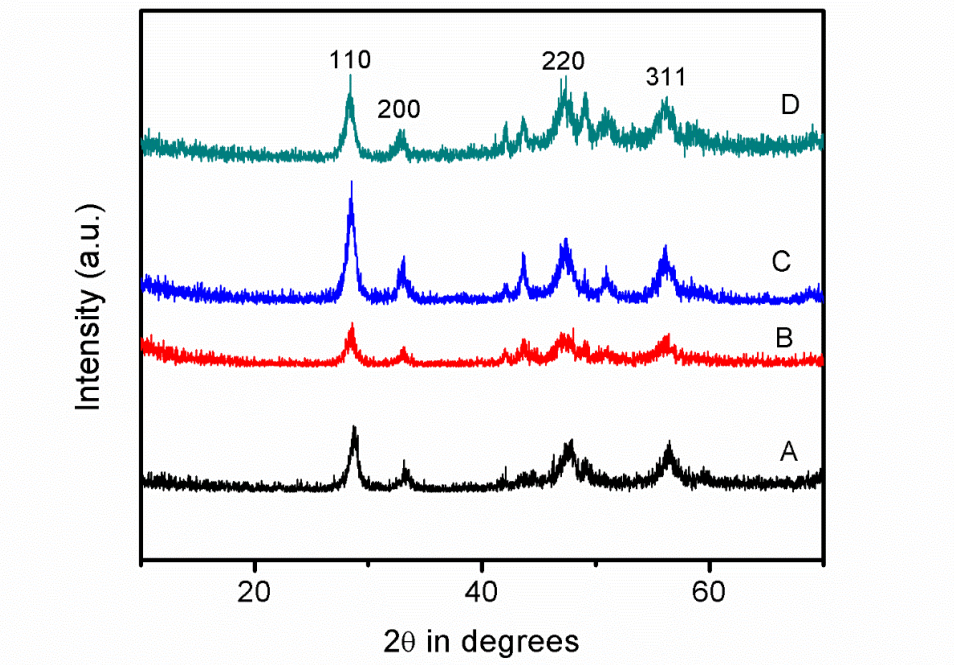

Figure 3: XRD pattern of A: Ce B:CS 101 C:CS 102 D:CS 103

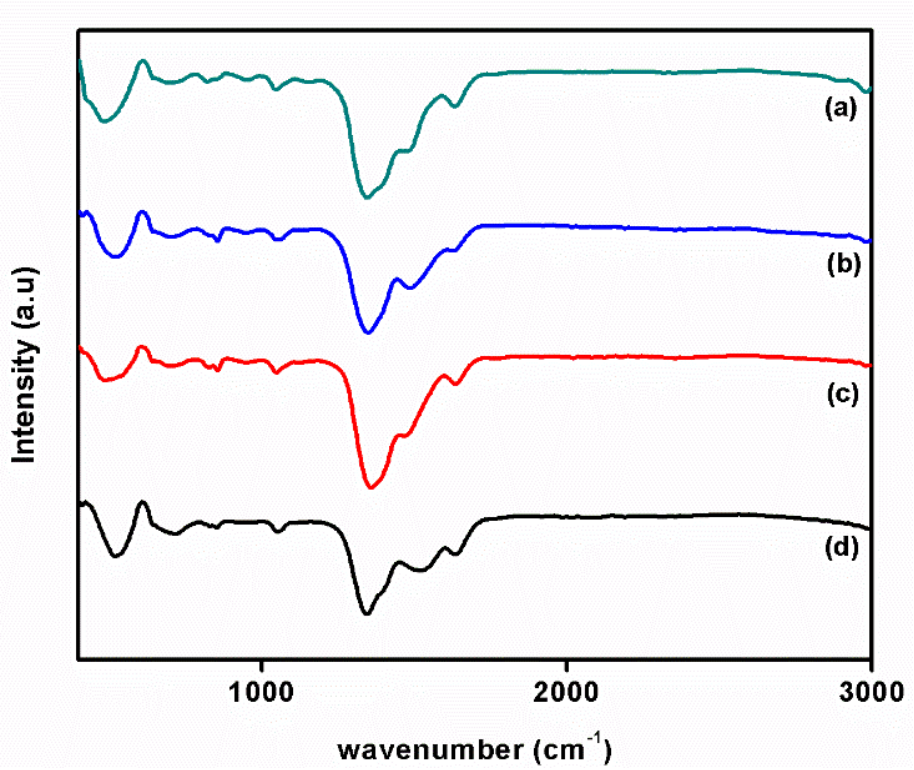

Figure 4a: FT-IR spectra of Ce using (a) Palak, (b) Palak leaf Ext, (c) Bay and (d) Plantain

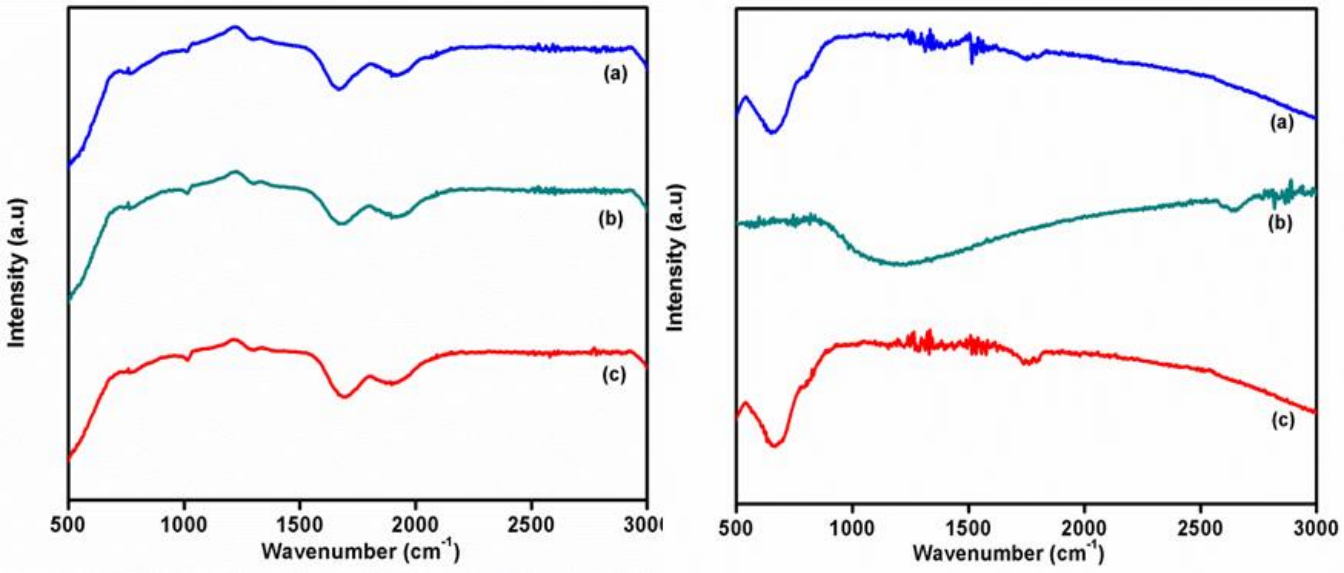

Figure 4b: FT-IR spectra of (a) CeLa1, (b) CeLa2, (c) CeLa3 and 4c: FT-IR spectra of (a) CeSm1, (b) CeSm2, (c) CeSm3

The FTIR spectra of CeO_2-Sm_2O_3 nanoparticles given in figure 4 shows the types of bonds present in it. The broad band at 3470.5 cm^{-1} corresponds to the O-H vibrations of the attached water molecules on the nanoparticle surface. The IR band below 700 cm^{-1} arises due to the stretching frequency of Ce-O bond. The FTIR peaks at around 1374.1, 1047.6 cm^{-1} may be due to the coordinated CO_2 molecules on the particle surface.

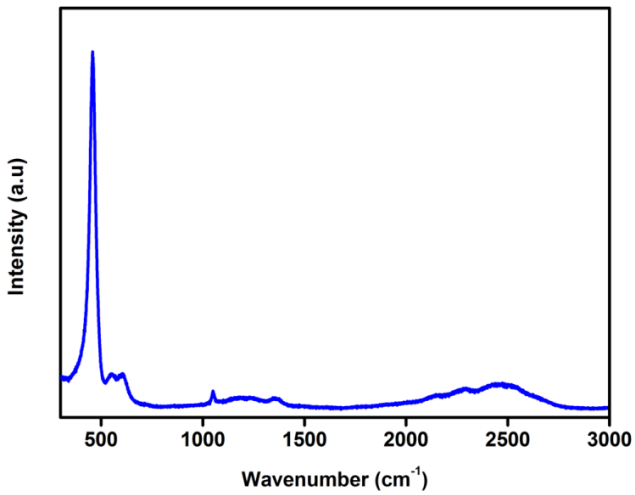

Figure 5. Raman Spectrum of CeO_2 (C100)

The cubic structure of CeO_2 is further confirmed by Raman Spectroscopy (Figure 5). The Raman spectrum of the sample shows prominent broad peak at 461.2 cm^{-1} that correspond to the symmetrical vibrations of Ce-O vibrational unit. There are symmetrical vibrations of the oxygen atoms around each cation. The vibrations are almost independent of cation mass as only the oxygen atoms vibrate. Further, SEM and EDAX analysis of the prepared samples shows (Figure 6) the surface morphology and the elements present in it. For the modified samples the EDX values are very close to the expected values. Most of the SEM images show agglomerated particles of cerium oxide.

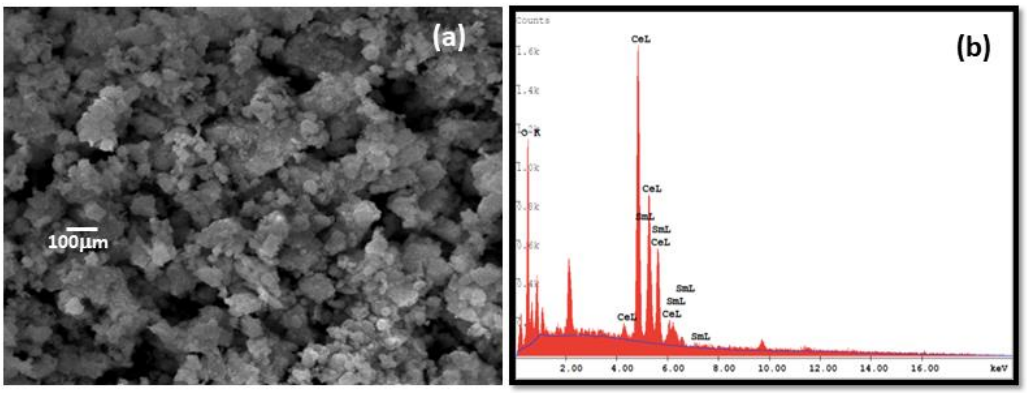

Figure 6: (a) SEM image and (b) EDAX spectrum of Sm_2O_3/CeO_2

The TGA curve shows (Figure 7) that there is a steady mass loss from 30^0C to 200^0C due to the escape of moisture and adsorbed CO_2 present [71]. The small drop in mass from 200^0C to 500^0C may correspond to the loss of phytochemical substances present in the leaf extract. The mass becomes constant with temperature till 1000^0C. The total weight loss up to 1000^0C is around 8% of the total mass. There is no decomposition of the sample till 1000^0C which explains that the catalysts can be used for higher temperature applications. The DSC plot of the sample indicates the absence of any phase transformation taking place during the temperature rise.

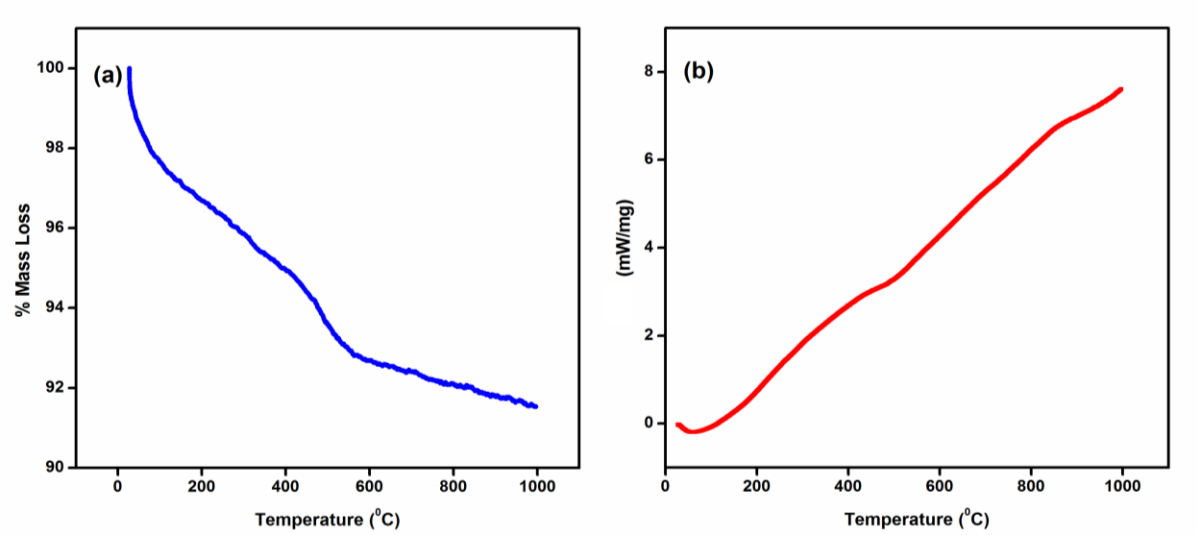

Figure 7: (a) TGA curve, (b) DSC curve for Sm_2O_3/CeO_2 sample

The optical catalytic activity and the photodegradation activity of the catalyst depends on the band gap of the material used. For CeO_2 band gap energy is found to be 3.03 eV. Modified sample the band gap energy is found to be less compared to pure ceria. In the case of Sm_2O_3/CeO_2 sample the band gap energy (Figure 8) is calculated using Tauc plot and is found to be 2.6 eV. This value indicate that the material can be used in the photocatalysis in presence of UV/visible light.

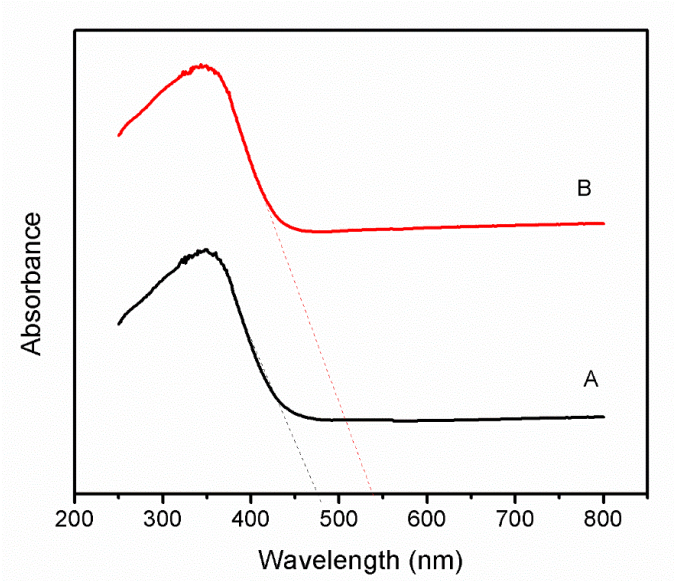

Figure 8: UV-DRS spectra of (A) CeO_2 and (B) Sm_2O_3/CeO_2

TEM image (Figure 9) of one of the representative samples has been studied and is given here. The CeO_2-Sm_2O_3 shows a sharp electron diffraction pattern indicating a high degree of crystallinity as already confirmed by the XRD analysis. The marked area in the micrographs reveals the closer view of the particle ensemble and orientation of the crystallographic planes (111).

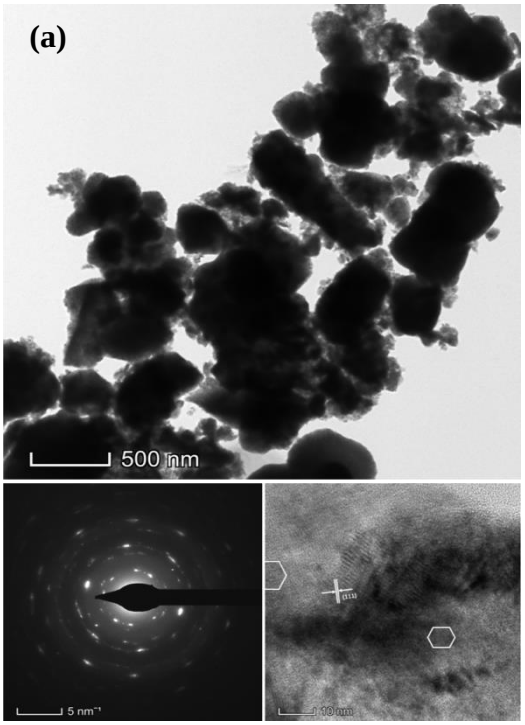

Figure 9: TEM image of CeO_2 catalyst

DLS study reveals that ceria is not in nanorange. The diameter varies between 500 to 1000 nm range. This could be due to the agglomeration after the nanoparticles were synthesized. XPS spectra has been studied for (CT101) Ce/TiO_2 catalyst. In Ce/TiO_2, spin orbital components of Ti were observed at 460.1 eV (Ti2p3/2) and 465.5 eV (Ti2p1/2). Shift of these peaks towards higher binding energy values compared to pure TiO_2 shows the incorporation Ce^{4+} into titania lattice. Lattice oxygen was observed as a shoulder at 529 eV and the peak at 531.6 eV indicates the presence of surface hydroxyl group. The labelled peaks are assigned to the spin-orbital the incorporation into the titania lattice splitting components of Ce3d levels.

The spin-orbit multiplets and the peak at 917 eV confirmed existence of Ce4+ and its incorporation into the TiO_2 lattice.

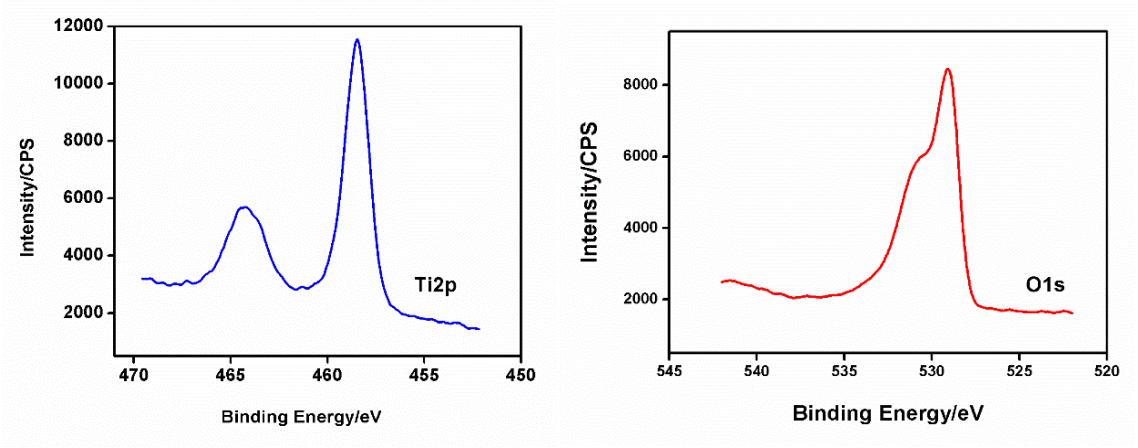

Figure 10: XPS spectrum of O1s level of TiO_2 and Ce/TiO_2

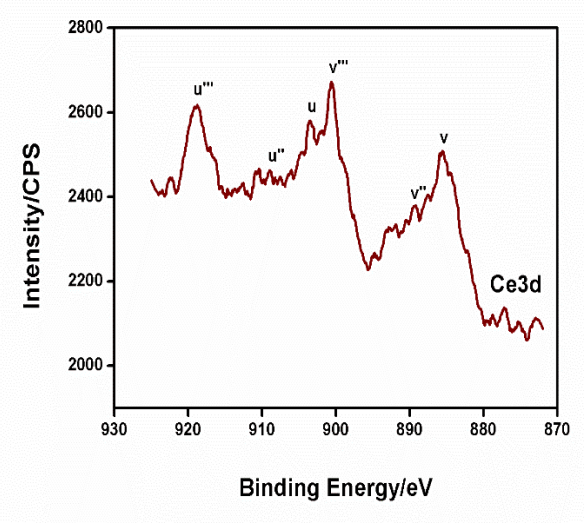

Figure 11: XPS spectrum of Ce 3d levels of Ce/TiO_2

5.2. Catalytic Reactions under study

5.2.1.Photodegradation of Malachite green dye

Malachite green (Figure 12) is the common name for an industrial dye having IUPAC name 4-[(4-dimethylaminophenyl)- phenyl-methyl]-N, N-dimethyl aniline and is a toxic chemical. It is also known as basic green 4, diamond green B, aniline green, and Victoria green. The photocatalytic degradation process of the dye in initiated by the photoexcitation of the nanoparticles. Electron-hole pairs are formed on the surface of the catalyst when light of suitable energy falls on it. Electrons from the conduction band are utilized by the dissolved oxygen to form oxygen radical ions ($O^{2\cdot-}$). The oxygen radical ions are a very reactive and are capable of oxidizing dye molecules. The high oxidative potential of the holes (h+) present in the valence band of the catalyst on irradiation enables the oxidation of the dye and thereby culminating in its degradation [72] .Various reaction parameters were studied to optimize the reaction conditions.

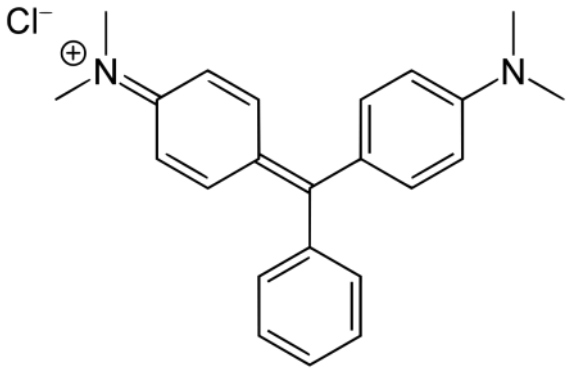

Figure 12: Structure of Malachite green

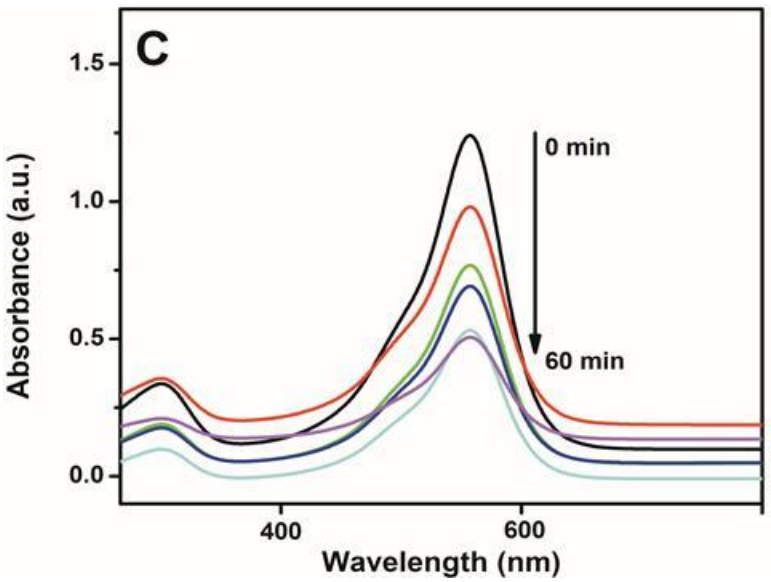

Figure. 13. Photodegradation of MG using CeO_2 prepared from spinach leaf

The photodegradation efficiency of MG was carried out for a time of 60 minutes (Figure 13). The initial concentration of dye was taken at 15 mg/L and that of the amount of catalyst at 30 mg/100 mL. The amount of catalyst was kept constant throughout the trials. Degradation reaction was studied under visible light and a neutral pH. The degradation efficiency increases with the progress of time, which can be attributed to the increase in the formation of $O^{2\bullet}$ and •OH. As more light energy falls on the catalyst with the increase in irradiation time a proportionate increase in the formation of photoexcited species is observed which enhances the photocatalytic activity (Table 3).

Table 3: % Photodegradation of different CeO_2 system for one hour using 0.3g catalyst

Catalyst	degradation of MG (%)
Plantain leaf	55 %
Bay leaf	57 %
Spinach leaf	64 %
Spinach extract	62 %

Better degrdation was obtained for the catalyst prepared using spinach leaf. Catalyst reusablility has been studied for this reaction and is found that it can be used till 4 cylces without much change in the conversion.

Note: The MG dye degradation studies were done for C100 catalyst system prepared with different plants and extracts. Further MG degradation studies were done for the C100, CS101,CS102,CS103, CL101,CL102,CL103 systems.

5.2.2. Photodegradation of Congo Red dye

In our present study, the efficiency of the catalyst was validated on the photodegradation of CR under simulated solar illumination. The degradation of CR under illumination was 12% in the absence of catalyst and no significant photodegradation occurred in the absence of sunlight even though catalyst was added. Studies were conducted by varying parameters such as dye concentration, catalyst dosage, time and pH. As the dye concentration changes the % degradation decreases as shown in the Table 4.

Optimization study for the photodegradation of CR was carried out by varying the amount of catalyst from 50 mg/L to 250 mg/L. The concentration of CR was maintained at 20mg/L and the pH at 3 and the study was conducted for a period of 1 hr in all cases. As had been the observation earlier, the rate of photodegradation increased in proportion to the amount of catalyst up to a point. Thereafter, the rate decreased even after increasing the amount of catalyst. The initial increase in the activity may be due to the increase in the number of active sites. The initial increase in the activity may be due to the increase in the number of active sites. After reaching an optimum value, further increase of catalyst dosage (>100 mg), adversely influenced the efficiency of degradation.

Table 4: Effect of CR concentration on photodegradation rate

Dye concentration (mg/L)	Degradation of CR dye (%)
	Ce/TiO_2
20	89.9
40	80.7
60	71.3
80	63.2
100	52.7

Reaction Conditions: Amount of the catalyst: 100 mg/L, Time:1 h, pH: 3

CR is a polynuclear aromatic molecule with two sulfonic groups and ionizes in the acidic medium and forms a soluble CR anion (Figure 14). These anions can easily adsorb onto the surface of the catalyst and undergoes photodegradation under solar irradiation. It has already been reported that under alkaline pH, a coulombic repulsion is created between negatively charged titania surface and the dye molecules, thereby decreasing the photoactivity [73]. Degradation studies were carried out only in the acidic pH under the optimized conditions (20 mg/L of the dye solution and 100 mg/L of the catalyst) for one hour. Maximum efficiency was found at a pH 3.0 for Ce/TiO_2. At higher pH values, a lesser amount of surface -OH groups were observed, which lead to a lower activity.

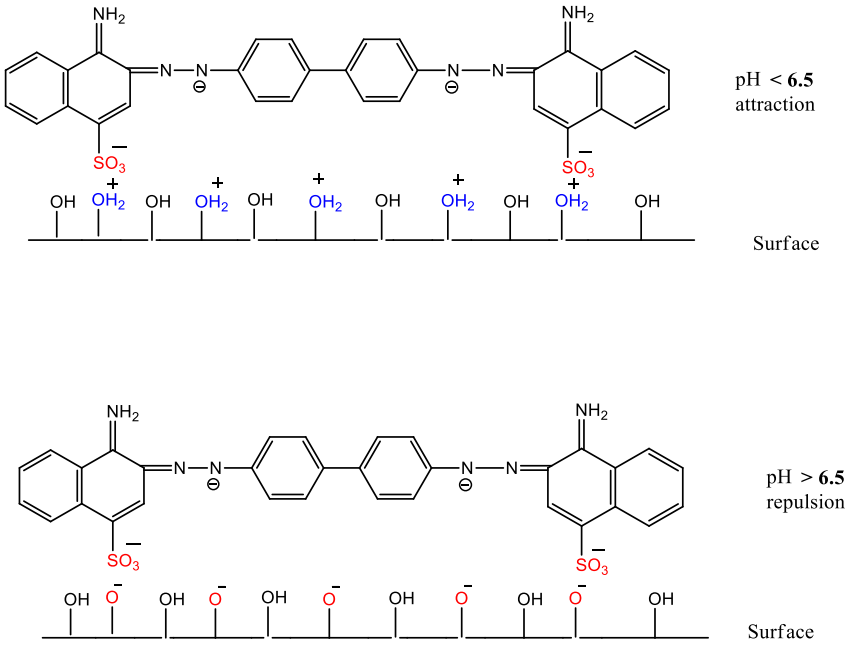

Figure.14: The interaction between titania surface and CR dye under acidic and basic pH

Langmuir-Hinshelwood (LH) kinetic model (Eq. 6) was used to explain the degradation kinetics of dyes in the presence of heterogeneous photocatalysts[74].Under low dye concentrations, the integrated LH equation shifts to a pseudo-first-order kinetic equation (Eq. 7).

$$r_0 = -\frac{d\,[C_0]}{dt} = \frac{k_{LH}K_{ads}[C_0]}{1 + K_{ads}[C_0]} \tag{6}$$

$$t = \frac{1}{k_{LH}K_{ads}} ln\frac{[C_0]}{[C]} \tag{7}$$

Where k_{LH} is the rate constant of the reaction, K_{ads} is the rate of dye adsorption on the surface of the photocatalyst, $[C_0]$ and $[C]$ dye concentrations at the beginning and time *t*, respectively. A plot of $ln\frac{[C_0]}{[C]}$ versus t gives k_{app}. The rate of dye degradation decreases with increase in dye concentration, which is in accordance with Langmuir–Hinshelwood kinetic model (Figure 15).

Catalyst reusablility has been studied for this reaction and is found that it can be used til 4 cylces without much change in the conversion.

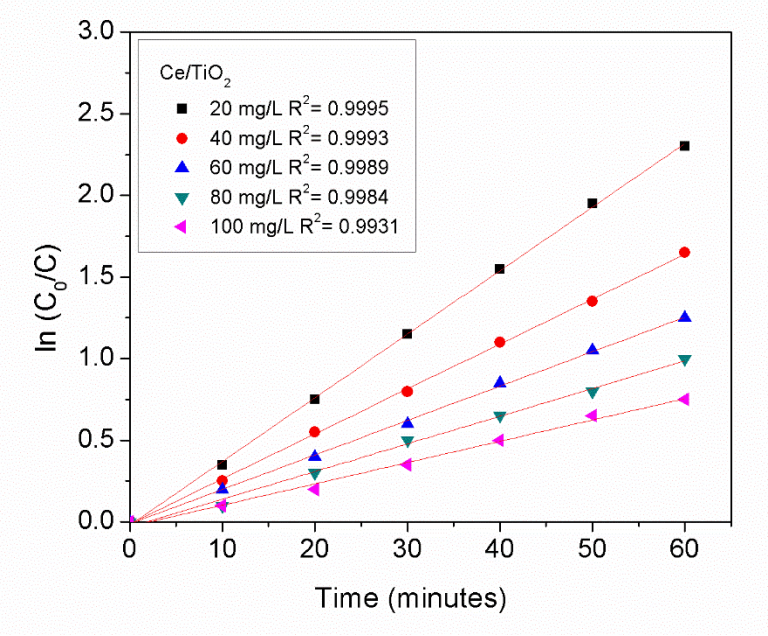

Figure.15: Plot of ln C_0/C vs time

Note: Congo Red (CR) dye degradation studies were performed for all Samaria and all lanthana doped catalyst systems of Ce, viz., C100, CS101,CS102,CS103, CL101,CL102,CL103 systems.

5.2.3. Degradation of ciprofloxacin

The ciprofloxacin (Figure 16) was chosen as a model to observe the degradation of fluoroquinolones in an aqueous medium.

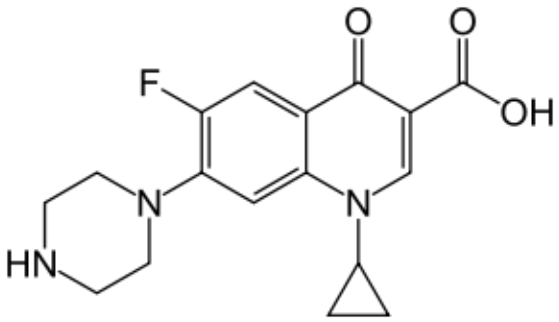

Figure 16: structure of Ciprofloxacin

The study of degradation of ciprofloxacin shows (Table 5) that the maximum degradation was observed for the CS101 and the best results were obtained when the catalyst loading was 0.03 g catalyst over a period of 2 hours and for a concentration of 3 µM sample of the drug (Figure 17).

Table 5: Effect of amount of catalyst on ciprofloxacin degradation

Amount of catalyst (g)	% degradation of CIP
0.01	35
0.02	56
0.03	65
0.04	53
0.05	45

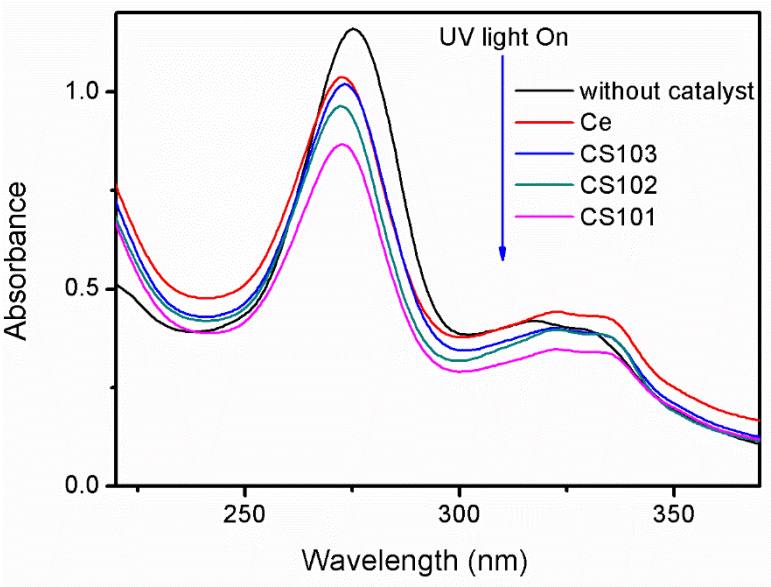

Figure. 17: Degradation of ciprofloxacin under uv light.

Table 6: Percentage of degradation of ciprofloxacin with various catalysts

Sl. No.	Catalyst	Degradation of CIP (%)
1	Ce	11.4
2	CeSm3	18.4
3	CeOLa3	15.8
4	CeSmLa	19.5
5	CeZn	34.3
6	CegCN	28.2
7	CeAg	38.3
8	CegCNAg	63.5

Percentage degradation of different catalytic system are given in Table 6. Catalyst reusablility has been studied for this reaction and is found that it can be used for upto 4 cylces without much change in the conversion rate.

Note: Ciprofloxacin (CIP) degradation studies were performed for all Samaria and all lanthana doped catalyst systems of Ce, viz., C100, CS101,CS102,CS103, CL101,CL102,CL103 systems.

5.2.4. Reduction of 4 Nitrophenol

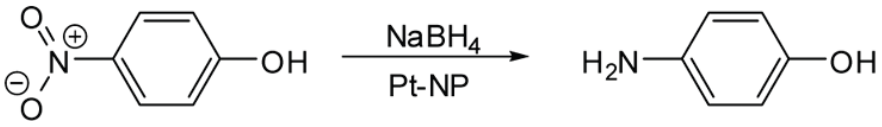

Figure 18: Scheme for 4 NP degradation

The schematic representation of 4NP reduction is shown in Figure 18. The catalytic reduction of 4-NP is carried out in aqueous medium using sodium borohydride and required amount of catalyst (Figure 19).

The 4-ntrophenolate ion in the solution shows an absorption band at 400 nm. As the catalytic reaction proceeds, the absorption of the solution at 400 nm gets reduced (Figure 22). From this data we can plot the first order kinetic graph for the reduction of 4-nitrophenol.

$$\ln(C_0/C_t) = kt \quad (8)$$

Where C_0 and C_t represents absorbance at time 0 and t minutes respectively. Figure 8 shows good correlation with first order kinetics as the regression coefficient is found to be R^2=0.99. This plot confirms that the catalytic reduction of 4-nitrophenol follows pseudo first order kinetics (Figure 21).

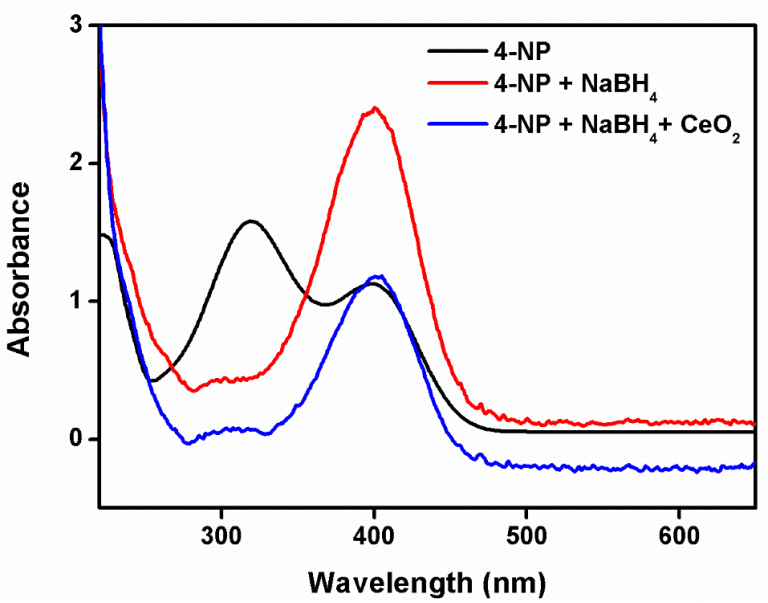

Figure 19: reaction of 4-NP reduction

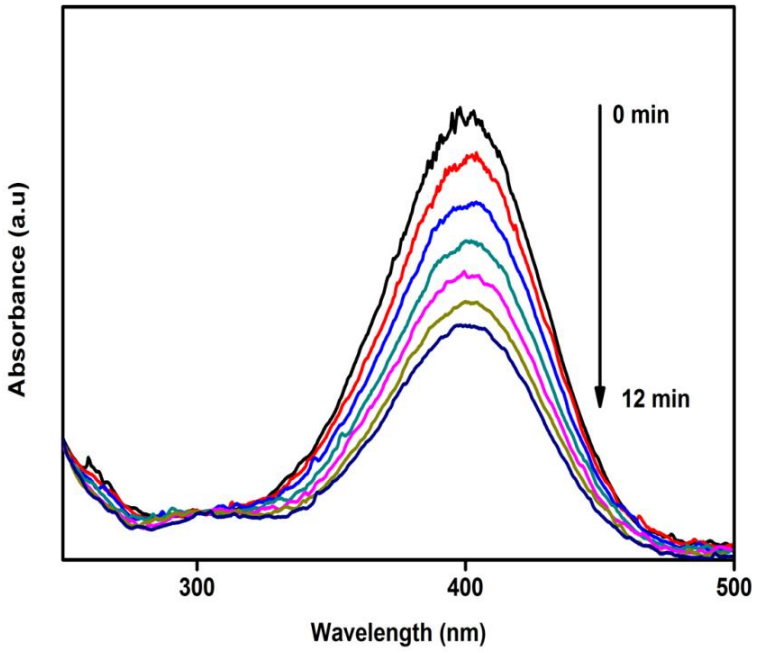

Figure. 20: Reduction of 4-NP using Sm_3O_4/CeO_2 catalyst

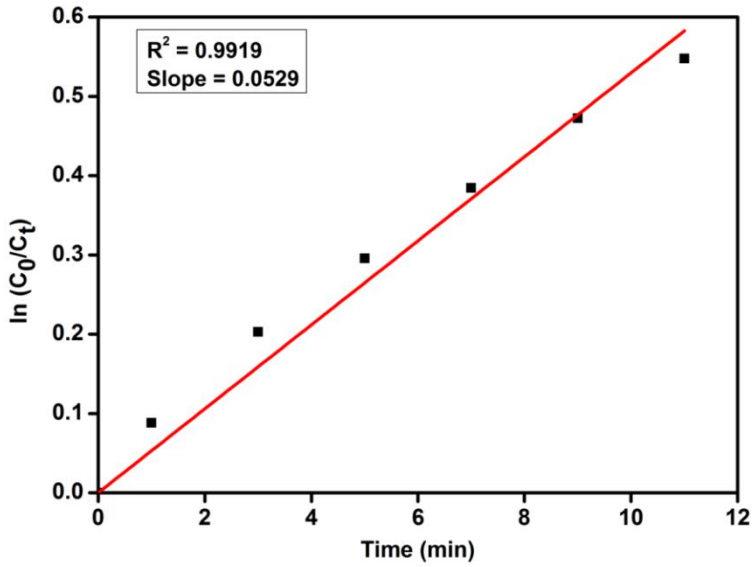

Figure 21: Kinetic study of the 4-NP reduction reaction

In the presence of the prepared catalyst, BH_4^- ions gets adsorbed to the catalyst surface (S). The electrons released upon oxidation of BH_4^- get transferred to the catalyst. This is used to generate hydrogen by the reduction of water. This gets adsorbed (dissociative adsorption) on the catalyst

surface to produce active hydrogen species which in turn converts 4-nitrophenol (4-NP) to 4-aminophenol (4-AP). Finally the whole catalytic cycle ends with the desorption of the product from the catalytic surface [75]. The plausible mechanism in Figure 22.

The stability and reusability of the catalysts was studied by reusing the catalyst for the same reaction under the optimized condition. A good catalyst must be stable and reusable at least up to 2-3 cycles. After the catalytic reaction, the catalyst was isolated, washed, dried and activated for further use. The experimental results show that CeO_2-Sm_2O_3 nanocomposite is stable and reusable catalyst up to 3 cycles without much loss in efficiency Figure 14. CeO_2-Sm_2O_3showed no notable change in the efficiency up to 3rd cycle but drastic change afterwards. Therefore CeO_2-Sm_2O_3 is an efficient, stable and economic catalyst for the catalytic reduction of organic pollutants.

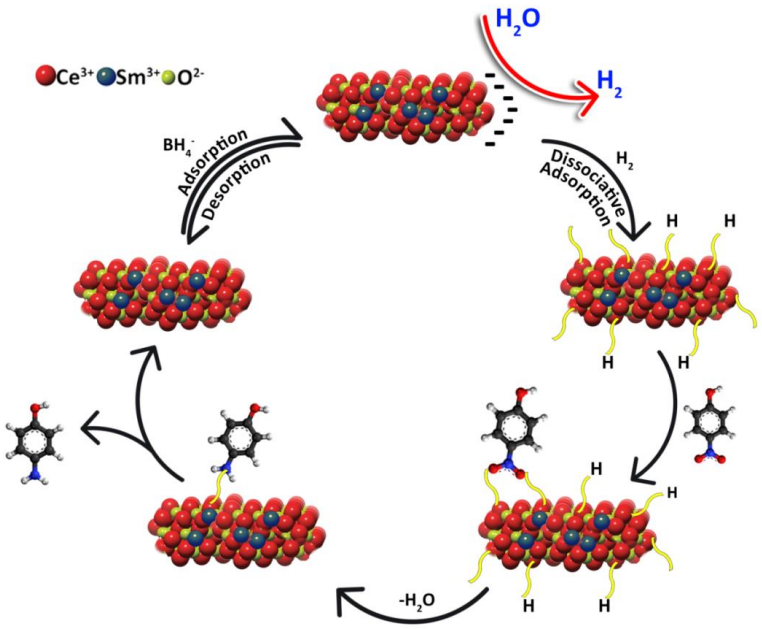

Figure 22: Mechanism of reduction of 4-NP

Note: Reduction of 4NP studies were performed for all Samaria and all lanthana doped catalyst systems of Ce, viz., C100, CS101,CS102,CS103, CL101,CL102,CL103 system.

5.2.5.Biginelli reaction

The product yield of Biginelli products were measured. The observation is tabulated in Table 7. As indicated by the table, the highest yield is obtained with the catalyst Ce-Zn. The catalyst was retrieved completely after washing the obtained product in water, dissolving the product in ethyl acetate, filtering it and using rotavapor to vaporize the solvent. The product can be scraped from the round bottom flask and ground into a powder before storing it into air-tight containers.

Table 7: Yield of products in Biginelli reaction

Catalyst	Yield (%)
Ce	47.3
CeSm3	68.3
CeLa3	52.4
CeSmLa	57.4
CeZn	74.5
CeTi	63.8
CegCN	54.7
CegCNAg	58.5

5.3. Statistical Analysis of the data obtained from Box-Behnken Design

The statistics package named Minitab developed at the Pennsylvania State University is used to create contour plots in the second dimension and response surface plots in the third dimension, which are basically plots of the response of the reaction studied with respect to different reaction parameters that influence the response of the reaction. In the experimental model that we have, the conversion % of 4-NP is studied as a function with four distinctive inputs, namely a) Concentration of 4-NP, b) Time, c) Amount of the catalyst and d) Concentration of sodium borohydride.

According to BBD design, 27 different runs were performed, all in duplicates to get precise results. FITS value from the experimental design was obtained after incorporating these results, and the significance of this model is confirmed by the ANOVA method for analysis of variance. There no significant difference between the experimental and predicted values and thus confirms the accuracy of the model. The Statistical study presented here is done based on a regression equation, which is a polynomial equation in several variables that expresses the linear relationship between various input parameters on the reduction of 4-NP. The contour and surface plot of the reaction is given in Figure 23 and 24 respectively.

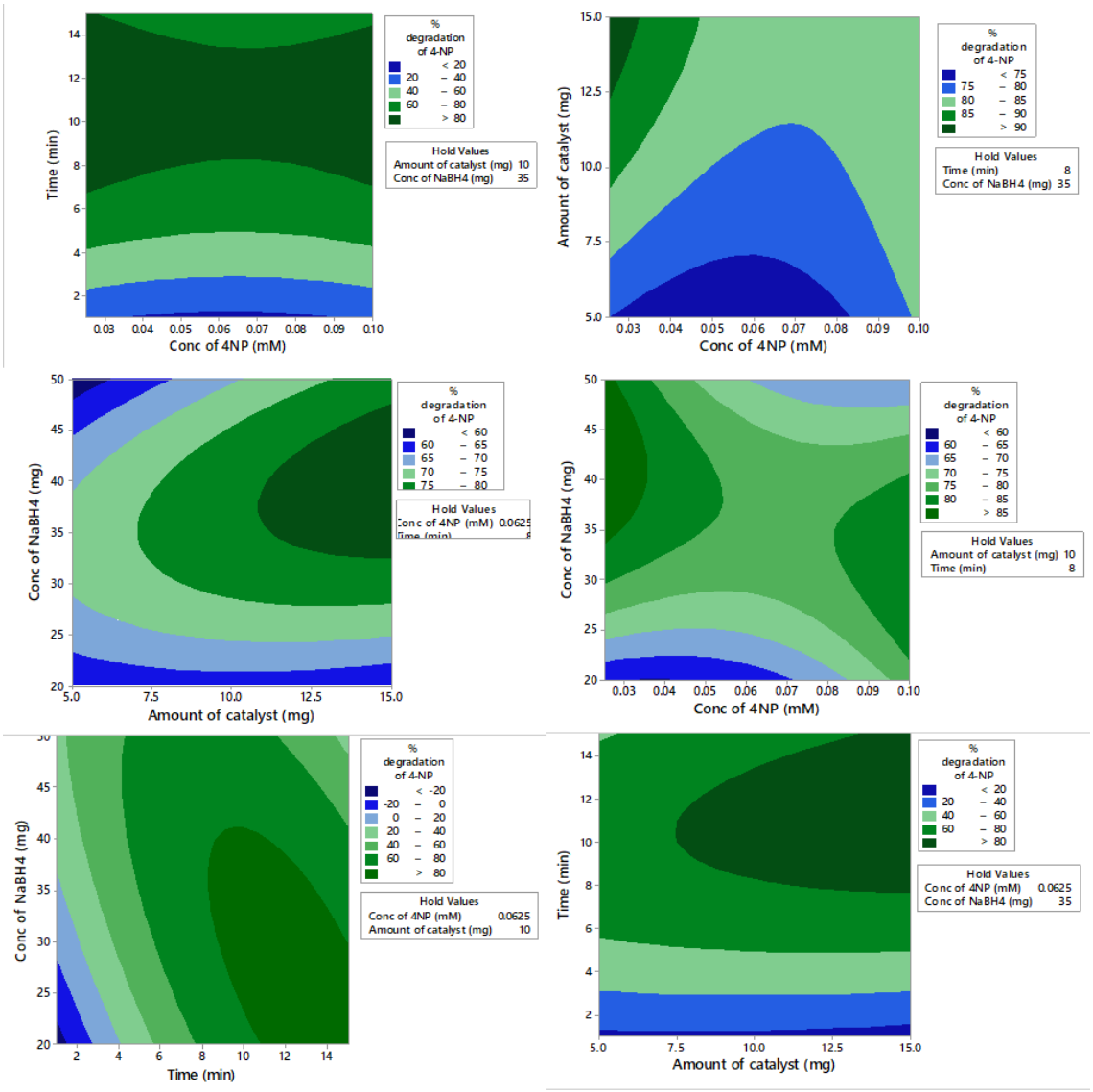

Figure 23. Contour plot for the interaction of various reaction parameters

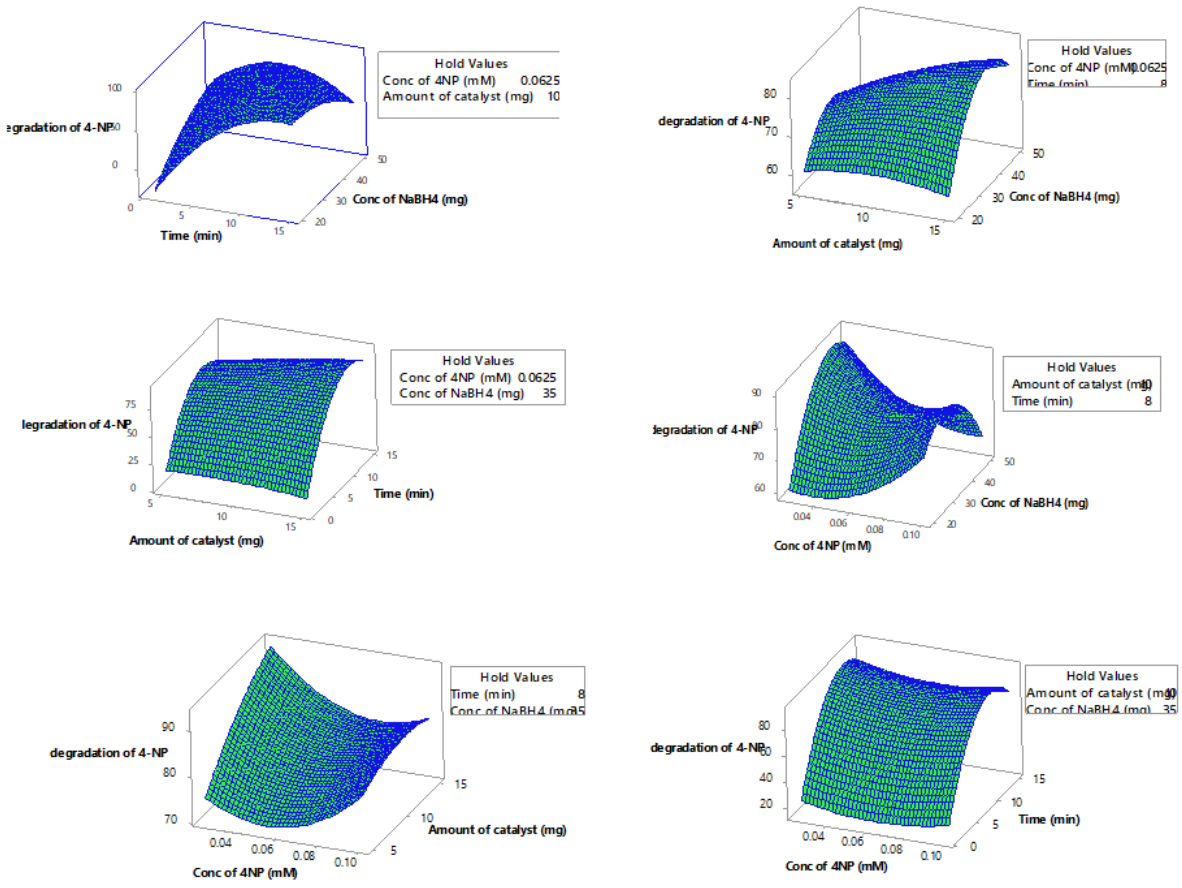

Figur 24. Surface plot for the interaction of various reaction parameters

6. SUMMARY AND CONCLUSION

- A set of catalysts were prepared by the solution combustion synthesis using the biogenic synthetic route. The catalysts were all based on ceria and ceria modified using other metal oxides/metal. The prepared catalysts were characterized using techniques like XRD, FTIR, SEM, TEM, Raman spectroscopy and TGA/DSC. The prepared catalysts were then studied for their catalytic efficiency.
- The prepared catalysts were studied for their ability to degrade the dyes malachite green and Congo red. Their ability to degrade an antibiotic which is widely present in water bodies, namely ciprofloxacin was studied.
- The prepared catalysts were exploited for their ability to reduce 4 nitrophenol and the catalyst system where ceria modified with samarium was found to be the best.
- The catalyst was utilized for the synthesis of a series of aldehydes for the Biginelli synthesis. The catalysts were found to be effective in catalyzing the reaction.

Structure of Thesis

The thesis will be made up of 9 Chapters.

Chapter 1. Introduction. All the topics pertaining to the thesis will be briefly introduced. The need for the study will also be mentioned at the end.

Chapter 2. Review of literature. The literature pertaining to the topics will be reviewed in order to establish the relevance of the work and also to put the work in perspective. By the end of the chapter, the aims and objectives will be mentioned.

Chapter 3. Materials and Methods. This chapter will discuss the materials used as well as the methodology, both experimental and instrumental. A brief discussion on all the instrumental methods used for characterization of the catalyst will be incorporated.

Chapter 4. Result and discussion. The results of the instrumental methods used for characterization of the catalysts will be presented here and the relevant discussions, analyses, and conclusions drawn from them will be discussed.

Chapter 5. Photocatalytic degradation . This chapter will discuss the photodegradation studies of the two dyes Malachite green and Congo red as also the degradation of the antibiotic drug, Ciprofloxacin.

Chapter 6. Reduction of 4-Nitrophenol. This chapter will deal with the catatytic reduction of 4-Nitrophenol using the catalysts prepared.

Chapter 7. Biginelli reactions. This chapter will have the discussion of the compounds synthesized using the Biginelli reaction.

Chapter 8. Statistical analysis. Two studies done earlier, reduction of 4-Nitrophenol and degradation of Ciprofloxacin will be statistically analyzed using the Response Surface Methodology based on the Box Behnken Design.

Chapter 9. This chapter will summarize the entire work and give the concluding remarks.

REFERENCES

[1] M. Bettinelli, L. Carlos, and X. Liu, "Lanthanide-doped upconversion nanoparticles," *Phys. Today*, vol. 68, no. 9, pp. 38–44, 2015.

[2] Z. Wang and R. Yu, "Hollow Micro/Nanostructured Ceria-Based Materials: Synthetic Strategies and Versatile Applications," *Adv. Mater.*, vol. 1800592, pp. 1–34, 2018.

[3] A. TROVARELLI, "Catalytic Properties of Ceria and CeO_2 -Containing Materials," *Catal. Rev.*, vol. 38, no. 4, pp. 439–520, 1996.

[4] X. Wang, Y. Ma, S. Li, A. H. Kashyout, B. Zhu, and M. Muhammed, "Ceria-based nanocomposite with simultaneous proton and oxygen ion conductivity for low-temperature solid oxide fuel cells," *J. Power Sources*, vol. 196, no. 5, pp. 2754–2758, 2011.

[5] C. E. Castano, M. J. O'Keefe, and W. G. Fahrenholtz, "Cerium-based oxide coatings," *Curr. Opin. Solid State Mater. Sci.*, vol. 19, no. 2, pp. 69–76, 2015.

[6] C. Xu and X. Qu, "Cerium oxide nanoparticle: a remarkably versatile rare earth nanomaterial for biological applications," *NPG Asia Mater.*, vol. 6, no. 3, pp.90, 2014.

[7] A. Corma, P. Atienzar, H. García, and J.-Y. Chane-Ching, "Hierarchically mesostructured doped CeO2 with potential for solar-cell use," *Nat. Mater.*, vol. 3, no. 6, pp. 394–397, 2004.

[8] P. Patsalas, S. Logothetidis, and C. Metaxa, "Optical performance of nanocrystalline transparent ceria films," *Appl. Phys. Lett.*, vol. 81, no. 3, pp. 466–468, 2002.

[9] P. Jasinski, T. Suzuki, and H. U. Anderson, "Nanocrystalline undoped ceria oxygen sensor," *Sensors Actuators, B Chem.*, vol. 95, no. 1–3, pp. 73–77, 2003.

[10] S. Lee, Z. Lu, S. V Babu, and E. Matijevic, "Chemical mechanical polishing of thermal oxide films using silica particles coated with ceria," vol. 5814, no. 3, 2002.

[11] A. Dhall and W. Self, "Cerium Oxide Nanoparticles : A Brief Review of Their Synthesis Methods and Biomedical Applications," *Biotechnol. Reports 17*, pp. 1–13, 2018.

[12] S. Rajeshkumar and P. Naik, "Synthesis and biomedical applications of Cerium oxide nanoparticles – A Review," *Biotechnol. Reports*, vol. 17, pp. 1–5, 2018.

[13] M. Lykaki *et al.*, "Ceria nanoparticles shape effects on the structural defects and surface chemistry: Implications in CO oxidation by Cu/CeO_2catalysts," *Appl. Catal. B Environ.*, vol. 230, no. 2010, pp. 18–28, 2018.

[14] B. Elahi, M. Mirzaee, M. Darroudi, R. Kazemi Oskuee, K. Sadri, and M. S. Amiri, "Preparation of cerium oxide nanoparticles in Salvia Macrosiphon Boiss seeds extract and investigation of their photo-catalytic activities," *Ceram. Int.*, vol. 45, no. 4, pp. 4790–4797, 2019.

[15] I. Iglesias, M. Forti, G. Baronetti, and F. Mariño, "Zr-enhanced stability of ceria based

supports for methane steam reforming at severe reaction conditions," *Int. J. Hydrogen Energy*, no. xxxx, 2019.

[16] Z. Pászti, O. Hakkel, G. P. Szíjjártó, and A. Tompos, "Adsorption and transformations of ethanol over ceria based model catalysts," *Catal. Today*, vol. 306, pp. 145–153, 2018.

[17] M. J. Muñoz-Batista, A. M. Eslava-Castillo, A. Kubacka, and M. Fernández-García, "Thermo-photo degradation of 2-propanol using a composite ceria-titania catalyst: Physico-chemical interpretation from a kinetic model," *Appl. Catal. B Environ.*, vol. 225, pp. 298–306, 2018.

[18] Y. Tang, S. Ma, W. Chen, X. Li, and L. Li, "Catalytic Ozonation of Ciprofloxacin over Cerium Oxide Modified SBA-15 and Toxicity Assessment towards *E. coli*," *J. Adv. Oxid. Technol.*, vol. 21, no. 1, pp. 159–169, 2018.

[19] J. Weng *et al.*, "Ceria-based nanoflake arrays integrated on 3D cordierite honeycombs for efficient low-temperature diesel oxidation catalyst," *Appl. Catal. B Environ.*, vol. 245, pp. 623–634, 2019.

[20] R. Magudieshwaran *et al.*, "Green and chemical synthesized CeO_2 nanoparticles for photocatalytic indoor air pollutant degradation," *Mater. Lett.*, vol. 239, pp. 40–44, 2019.

[21] C. Pizzolitto *et al.*, "Increase of Ceria Redox Ability by Lanthanum Addition on Ni Based Catalysts for Hydrogen Production," *ACS Sustain. Chem. Eng.*, vol. 6, no. 11, pp. 13867–13876, 2018.

[22] I. V. Zagaynov, A. V. Naumkin, and Y. V. Grigoriev, "Perspective intermediate temperature ceria based catalysts for CO oxidation," *Appl. Catal. B Environ.*, vol. 236, no. 2010, pp. 171–175, 2018.

[23] P. Cheviron, F. Gouanv, and E. Espuche, "Green synthesis of colloid silver nanoparticles and resulting biodegradable starch/silver nanocomposites," *Carbohydr. Polym.*, vol. 108, no. 1, pp. 291–298, 2014.

[24] J. L. Gardea-Torresdey, E. Gomez, J. R. Peralta-Videa, J. G. Parsons, H. Troiani, and M. Jose-Yacaman, "Alfalfa sprouts: A natural source for the synthesis of silver nanoparticles," *Langmuir*, vol. 19, no. 4, pp. 1357–1361, 2003.

[25] V. Polshettiwar and R. S. Varma, "Green chemistry by nano-catalysis," *Green Chem.*, vol. 12, no. 5, p. 743, 2010.

[26] T. J. Beveridge and R. G. E. Murray, "Sites of metal deposition in the cell wall of Bacillus subtilis," *J. Bacteriol.*, vol. 141, no. 2, pp. 876–887, 1980.

[27] T. Klaus-Joerger, R. Joerger, E. Olsson, and C. G. Granqvist, "Bacteria as workers in the living factory: Metal-accumulating bacteria and their potential for materials science," *Trends Biotechnol.*, vol. 19, no. 1, pp. 15–20, 2001.

[28] K. B. Narayanan and N. Sakthivel, "Green synthesis of biogenic metal nanoparticles by terrestrial and aquatic phototrophic and heterotrophic eukaryotes and biocompatible agents," *Adv. Colloid Interface Sci.*, vol. 169, no. 2, pp. 59–79, 2011.

[29] N. I. Hulkoti and T. C. Taranath, "Biosynthesis of nanoparticles using microbes-A review," *Colloids Surfaces B Biointerfaces*, vol. 121, pp. 474–483, 2014.

[30] A. Patel, N. Arora, V. Pruthi, and P. A. Pruthi, *Biological treatment of pulp and paper industry effluent by oleaginous yeast integrated with production of biodiesel as sustainable transportation fuel*, vol. 142. Elsevier Ltd, 2017.

[31] V. Armendariz *et al.*, "Size controlled gold nanoparticle formation by Avena sativa biomass: Use of plants in nanobiotechnology," *J. Nanoparticle Res.*, vol. 6, no. 4, pp. 377–382, 2004.

[32] M. O. Montes *et al.*, "Anisotropic gold nanoparticles and gold plates biosynthesis using alfalfa extracts," *J. Nanoparticle Res.*, vol. 13, no. 8, pp. 3113–3121, 2011.

[33] J. L. Gardea-Torresdey *et al.*, "Formation and Growth of Au Nanoparticles in live side Live Alfalfa Plants," *Nano Lett.*, vol. 2, pp. 397–401, 2002.

[34] A. Primo, T. Marino, A. Corma, R. Molinari, and H. García, "Efficient visible-light photocatalytic water splitting by minute amounts of gold supported on nanoparticulate CeO2 obtained by a biopolymer templating method," *J. Am. Chem. Soc.*, vol. 133, no. 18, pp. 6930–6933, 2011.

[35] K. Kasinathan, J. Kennedy, M. Elayaperumal, M. Henini, and M. Malik, "Photodegradation of organic pollutants RhB dye using UV simulated sunlight on ceria based TiO2 nanomaterials for antibacterial applications," *Sci. Rep.*, vol. 6, no. 1, p. 38064, 2016.

[36] Y. Li *et al.*, "Coupling oxygen ion conduction to photocatalysis in mesoporous nanorod-like ceria significantly improves photocatalytic efficiency," *J. Phys. Chem. C*, vol. 115, no. 29, pp. 14050–14057, 2011.

[37] P. Bansal, N. Bhullar, and D. Sud, " Studies on photodegradation of malachite green using TiO 2 /ZnO photocatalyst ," *Desalin. Water Treat.*, 2010.

[38] S. Meena, D. Vaya, and B. K. Das, "Photocatalytic degradation of Malachite Green dye by modified ZnO nanomaterial," *Bull. Mater. Sci.*, vol. 39, no. 7, pp. 1735–1743, 2016.

[39] C. Dushkin, S. Vassilev, V. Blaskov, N. Kaneva, Y. Dimitriev, and I. Stambolova, "Photocatalytic activity of nanostructured ZnO films prepared by two different methods for the photoinitiated decolorization of malachite green," *J. Alloys Compd.*, vol. 500, no. 2, pp. 252–258, 2010.

[40] P. Frid, S. V. Anisimov, and N. Popovic, "Congo red and protein aggregation in neurodegenerative diseases," *Brain Res. Rev.*, vol. 53, no. 1, pp. 135–160, 2007.

[41] T. An, H. Yang, G. Li, W. Song, W. J. Cooper, and X. Nie, "Kinetics and mechanism of advanced oxidation processes (AOPs) in degradation of ciprofloxacin in water," *Appl. Catal. B Environ.*, vol. 94, no. 3–4, pp. 288–294, 2010.

[42] S. Babić, M. Periša, and I. Škorić, "Photolytic degradation of norfloxacin, enrofloxacin and ciprofloxacin in various aqueous media," *Chemosphere*, vol. 91, no. 11, pp. 1635–1642, 2013.

[43] X. J. Wen, C. G. Niu, L. Zhang, C. Liang, H. Guo, and G. M. Zeng, "Photocatalytic degradation of ciprofloxacin by a novel Z-scheme CeO2–Ag/AgBr photocatalyst: Influencing factors, possible degradation pathways, and mechanism insight," *J. Catal.*, vol. 358, pp. 141–154, 2018.

[44] T. A. Gad-Allah, M. E. M. Ali, and M. I. Badawy, "Photocatalytic oxidation of ciprofloxacin under simulated sunlight," *J. Hazard. Mater.*, vol. 186, no. 1, pp. 751–755, 2011.

[45] J. Qian, Y. Xue, Y. Ao, P. Wang, and C. Wang, "Hydrothermal synthesis of CeO2/NaNbO3composites with enhanced photocatalytic performance," *Chinese J. Catal.*, vol. 39, no. 4, pp. 682–692, 2018.

[46] F. Nekouei, S. Nekouei, and H. Noorizadeh, "Enhanced adsorption and catalytic oxidation of ciprofloxacin by an Ag/AgCl@N-doped activated carbon composite," *J. Phys. Chem. Solids*, vol. 114, pp. 36–44, 2018.

[47] C. Liang, C. G. Niu, M. C. Shen, S. F. Yang, and G. M. Zeng, "Controllable fabrication of a novel heterojunction composite: AgBr and Ag@Ag2O co-modified Ag2CO3with excellent photocatalytic performance towards refractory pollutant degradation," *New J. Chem.*, vol. 42, no. 5, pp. 3270–3281, 2018.

[48] A. Rahmani-Aliabadi and A. Nezamzadeh-Ejhieh, "A visible light FeS/Fe2S3/zeolite photocatalyst towards photodegradation of ciprofloxacin," *J. Photochem. Photobiol. A Chem.*, vol. 357, pp. 1–10, 2018.

[49] L. Ganranoo *et al.*, "Measurement of nitrophenols in rain and air by two-dimensional liquid chromatography-chemically active liquid core waveguide spectrometry," *Anal. Chem.*, vol. 82, no. 13, pp. 5838–5843, 2010.

[50] H. U. Blaser, "A golden boost to an old reaction," *Science (80-.).*, vol. 313, no. 5785, pp. 312–313, 2006.

[51] S. Jana *et al.*, "Synthesis of silver nanoshell-coated cationic polystyrene beads: A solid phase catalyst for the reduction of 4-nitrophenol," *Appl. Catal. A Gen.*, vol. 313, no. 1–2, pp. 41–48, 2006.

[52] T. Aditya, A. Pal, and T. Pal, "Nitroarene reduction: A trusted model reaction to test nanoparticle catalysts," *Chem. Commun.*, vol. 51, no. 46, pp. 9410–9431, 2015.

[53] S. Wunder, F. Polzer, Y. Lu, Y. Mei, and M. Ballauff, "Kinetic analysis of catalytic reduction of 4-nitrophenol by metallic nanoparticles immobilized in spherical polyelectrolyte brushes," *J. Phys. Chem. C*, vol. 114, no. 19, pp. 8814–8820, 2010.

[54] Y. C. Chang and D. H. Chen, "Catalytic reduction of 4-nitrophenol by magnetically recoverable Au nanocatalyst," *J. Hazard. Mater.*, vol. 165, no. 1–3, pp. 664–669, 2009.

[55] X. Kong, H. Zhu, C. Le Chen, G. Huang, and Q. Chen, "Insights into the reduction of 4-nitrophenol to 4-aminophenol on catalysts," *Chem. Phys. Lett.*, vol. 684, pp. 148–152, 2017.

[56] X. K. Kong, Z. Y. Sun, M. Chen, C. Le Chen, and Q. W. Chen, "Metal-free catalytic

reduction of 4-nitrophenol to 4-aminophenol by N-doped graphene," *Energy Environ. Sci.*, 2013.

[57] J. Li, C. Liu, and Y. Liu, "Au/graphene hydrogel: synthesis, characterization and its use for catalytic reduction of 4-nitrophenol," *J. Mater. Chem.*, vol. 22, no. 17, p. 8426, 2012.

[58] M. V. Morales *et al.*, "Development of highly efficient Cu versus Pd catalysts supported on graphitic carbon materials for the reduction of 4-nitrophenol to 4-aminophenol at room temperature," *Carbon N. Y.*, vol. 111, pp. 150–161, 2017.

[59] A. Sharma, R. K. Dutta, A. Roychowdhury, D. Das, A. Goyal, and A. Kapoor, "Cobalt doped CuO nanoparticles as a highly efficient heterogeneous catalyst for reduction of 4-nitrophenol to 4-aminophenol," *Appl. Catal. A Gen.*, vol. 543, pp. 257–265, 2017.

[60] W. Shen *et al.*, "Catalytic reduction of 4-nitrophenol using gold nanoparticles biosynthesized by cell-free extracts of Aspergillus sp. WL-Au," *J. Hazard. Mater.*, vol. 321, pp. 299–306, 2017.

[61] Y. Yusran, D. Xu, Q. Fang, D. Zhang, and S. Qiu, "MOF-derived Co@N-C nanocatalyst for catalytic reduction of 4-nitrophenol to 4-aminophenol," *Microporous Mesoporous Mater.*, vol. 241, pp. 346–354, 2017.

[62] A. M. Zonouz and S. B. Hosseini, "Montmorillonite K10 clay: An efficient catalyst for Hantzsch synthesis of 1,4-dihydropyridine derivatives," *Synth. Commun.*, vol. 38, no. 2, pp. 290–296, 2008.

[63] C. O. Kappe, "Recent advances in the Biginelli dihydropyrimidine synthesis. New tricks from an old dog," *Acc. Chem. Res.*, vol. 33, no. 12, pp. 879–888, 2000.

[64] M. S. Holden and R. D. Crouch, "The Biginelli Reaction," *Multicomponent React.*, vol. 78, no. 8, pp. 1104–1105, 2005.

[65] F. Damkaci and A. Szymaniak, "Multicomponent heterocyclic chemistry for undergraduate organic laboratory: Biginelli reaction with multiple unknowns," *J. Chem. Educ.*, vol. 91, no. 6, pp. 943–945, 2014.

[66] M. Kidwai, S. Saxena, R. Mohan, and R. Venkataramanan, "A novel one pot synthesis of nitrogen containing heterocycles: An alternate methodology to the Biginelli and Hantzsch reactions," *J. Chem. Soc. Perkin 1*, vol. 2, no. 16, pp. 1845–1846, 2002.

[67] A. Debache, M. Amimour, A. Belfaitah, S. Rhouati, and B. Carboni, "A one-pot Biginelli synthesis of 3,4-dihydropyrimidin-2-(1H)-ones/thiones catalyzed by triphenylphosphine as Lewis base," *Tetrahedron Lett.*, vol. 49, no. 42, pp. 6119–6121, 2008.

[68] S. B. Khan, M. Faisal, M. M. Rahman, and A. Jamal, "Exploration of CeO_2 nanoparticles as a chemi-sensor and photo-catalyst for environmental applications," *Sci. Total Environ.*, vol. 409, no. 15, pp. 2987–2992, 2011.

[69] D. M. D. M. Prabaharan, K. Sadaiyandi, M. Mahendran, and S. Sagadevan, "Structural, Optical, Morphological and Dielectric Properties of Cerium Oxide Nanoparticles," *Mater. Res.*, vol. 19, no. 2, pp. 478–482, 2016.

[70] S. Phoka, P. Laokul, E. Swatsitang, and V. Promarak, “Synthesis , structural and optical properties of CeO 2 nanoparticles synthesized by a simple polyvinyl pyrrolidone (PVP) solution route,” vol. 115, pp. 423–428, 2009.

[71] K. K. Babitha, A. Sreedevi, K. P. Priyanka, B. Sabu, and T. Varghese, “Structural characterization and optical studies of CeO<inf>2</inf> nanoparticles synthesized by chemical precipitation,” *Indian J. Pure Appl. Phys.*, vol. 53, no. 9, pp. 596–603, 2015.

[72] A. Rajeswari, E. Jackcina Stobel Christy, and A. Pius, *New insight of hybrid membrane to degrade Congo red and Reactive yellow under sunlight*, vol. 179. Elsevier B.V, 2018.

[73] M. A. Rauf, M. A. Meetani, and S. Hisaindee, “An overview on the photocatalytic degradation of azo dyes in the presence of TiO_2 doped with selective transition metals,” *Desalination*, vol. 276, no. 1–3, pp. 13–27, 2011.

[74] K. R. Sunaja Devi, M. K. Mohan, D. Pinheiro, R. Rajan, A. Nizam, and S. Sugunan, “Investigation on the phase transformation and lattice parameters of Sn 2+ , Cu 2+ , La 3+ and Ce 4+ ions doped titania: characterization and solar light activity study,” *Optik (Stuttg).*, vol. 183, no. February, pp. 496–507, 2019.

[75] M. Kohantorabi and M. R. Gholami, “Kinetic Analysis of the Reduction of 4-Nitrophenol Catalyzed by CeO_2 Nanorods-Supported CuNi Nanoparticles,” *Ind. Eng. Chem. Res.*, vol. 56, no. 5, pp. 1159–1167, 2017.

LIST OF PUBLICATIONS AND PRESENTATIONS

Journal Publications

- Ajay Jose, K.R. Sunaja Devi, Dephan Pinheiro, S. Lakshmi Narayana, Electrochemical synthesis, photodegradation and antibacterial properties of PEG capped zinc oxide nanoparticles, Journal of Photochemistry and Photobiology B Biology. 187 (2018) 25–34, doi.org/10.1016/j.jphotobiol.2018.07.022.
- Kasinathan Karthik, K. R. Sunaja Devi, Dephan Pinheiro, and Sankaran Sugunan, Influence of Surfactant on the Phase Transformation of Bi_2O_3 and its Photocatalytic Activity Australian Journal of Chemistry. January 2019, /doi.org/10.1071/CH18446.
- K. R. Sunaja Devi, M. K. Mohan, D. Pinheiro, R. Rajan, A. Nizam, and S. Sugunan, “Investigation on the phase transformation and lattice parameters of Sn 2+ , Cu 2+ , La 3+ and Ce 4+ ions doped titania: characterization and solar light activity study,” *Optik (Stuttg).*, vol. 183, no. February, pp. 496–507, 2019.doi.org/10.1016/j.ijleo.2019.02.100.

- K Karthik, K R Sunaja Devi, Dephan Pinheiro Synthesis of bismuth silicate nanostructures with tunable morphology and enhanced photocatalytic activity, Indian Journal of Chemical Technology Vol. 26, March 2019 (Accepted).
- Dephan Pinheiro, K R Sunaja Devi, K Karthik, Ajay Jose and Sankaran Sugunan Phytogenic CeO_2-Sm_2O_3Nanocomposites with Enhanced Catalytic Activity for Reduction of 4-Nitrophenol Material research express (communicated).

Presentations (International & National Conferences)

- Pechmann Condensation over Cerium oxide Supported on Rice Husk Silica. 9th KSTA Annual conference on science and technology and innovations in the 21st Century, Dephan Pinheiro, Sunaja Devi K R during 20-21 December 2016 at Christ University, Bangalore.
- Bioinspired synthesis of ceria nano particles using *Ficus benghaiensis* (Indian Banyan) leaf extract and photocatalytic degradation of dye. Dephan Pinheiro, Sunaja Devi K R and Selvapriya.17-19/1/2018, "Proceedings of the 23rd National symposium on catalysis – CATSYMP-23" organized by Catalysis society of India during 17-20 January 2018, Bengaluru, India.
- Catalytic Reduction of 4-Nitrophenol using Phytogenic Sm_2O_3/CeO_2 Derived from *Spinacia oleracea*The International conference on "Proceedings of the International Conference of Nanoscience and Nanotechnology- ICONN2019" organized by SRMIST. Kattankulathur, Chennai. January 28-30, 2019.